A subtype of melanopsin ganglion cells encodes ground luminance

Michael H. Berry[1,2], Michael Moldavan[3,4], Tavita Garrett[1,5], Marc Meadows[5,6], Olga Cravetchi[3,4] Elizabeth White[1], Henrique von Gersdorff[1,2,6], Kevin M Wright[6], Charles Allen[3,4], Benjamin Sivyer[1,2,*]

1. Department of Ophthalmology, Casey Eye Institute

2. Department of Chemical Physiology and Biochemistry

3. Oregon Institute of Occupational Health Sciences

4. Department of Behavioral Neuroscience

5. Neuroscience Graduate program

6. Vollum Institute

Oregon Health & Science University, Portland, OR, 97239

* Corresponding author: sivyer@ohsu.edu

Abstract

Visual input to the hypothalamus from intrinsically photosensitive retinal ganglion cells (ipRGCs) influences several functions including circadian entrainment, body temperature, and sleep. ipRGCs also project to nuclei such as the supraoptic nucleus (SON), which is involved in systemic fluid homeostasis, maternal behavior, and appetite. However, little is known about the SON-projecting ipRGCs or their relationship to well-characterized ipRGC subtypes. Using a *GlyT2^{Cre}* mouse line, we identify a subtype of ipRGCs restricted to the dorsal retina that selectively project to the SON. These ipRGCs form a non-overlapping tiled mosaic that is limited to a dorsal region of the retina, forming a substrate for encoding ground luminance. Optogenetic activation of their axons demonstrates they release the neurotransmitter glutamate and that the SON is retinorecipient, receiving synaptic input from dorsal ipRGCs. Our results challenge the idea that ipRGC dendrites overlap to optimize photon capture and suggests non-image forming vision operates to sample local regions of the visual field.

Introduction

In addition to the rod and cone photoreceptors that are used for image-forming vision, the mammalian retina contains intrinsically photosensitive retinal ganglion cells (ipRGCs) that primarily drive non-image forming behaviors[1,2]. ipRGCs express their own photopigment, melanopsin[3], and project to a diverse array of central brain regions[4-6] influencing many homeostatic functions including circadian entrainment, pupil constriction, body temperature, sleep and mood[7-11]. There are six main *types* of ipRGCs (M1-M6), which are categorized according to their dendritic morphology, melanopsin expression, gene expression, and central projection locations[6,12]. The most studied of these, the M1 ipRGCs, have dendrites that occupy the OFF layer of the inner plexiform layer (IPL). They form the primary projections to the suprachiasmatic nucleus (SCN), which is the master circadian clock[7,13-16], and the shell of the olivary pretectal nucleus (OPN), which serves as the primary site of light dependent pupillary constriction[8,17,18]. They also project to a number of lateral hypothalamic brain regions, such as the supraoptic nucleus (SON), ventral lateral preoptic area (VLPO), and medial amygdaloid nucleus, though the functional role of these projections remains unclear[4,6,16].

The retinal responses of M1 ipRGCs are suited to their primary role in non-image forming vision; their long and sustained responses to bright illumination reflect their comparatively high expression of melanopsin and weak photoreceptor-mediated synaptic drive from retinal bipolar cells[6,19]. These light responses are optimal for signaling absolute light intensity and driving behaviors that are slow, such as circadian entrainment, and the maintained component of the pupillary light reflex[17,20,21]. M1 ipRGCs were first thought to comprise a single, homogenous population however, the discovery of a sub-population lacking *Brn3b* expression[18], the divergent projection patterns of M1 ipRGCs according to *Brn3b* expression [16,18], and the diversity of light responses within M1 ipRGCs[22,23] together suggest there are multiple M1 subtypes mediating different roles in non-image forming behavior.

The high density of M1 ipRGCs in the retina also suggests they comprise multiple subtypes. Conventional RGCs within a functional subtype are commonly arranged in evenly spaced mosaics where their dendrites form territories with minimal overlap[24,25].

This arrangement is thought to optimize the sampling of visual space[26-28] and reduces the encoding of redundant information, where each RGC subtype samples an even component of the visual field across the retina. Previous reports indicate M1 ipRGC dendrites are not territorial and they overlap considerably - about 4 fold[29] . This might be due to their non-image forming role, where the even representation of visual space is forgone in favor of increasing their dendritic surface area, thus maximizing the surface area for photon capture. Alternatively, they might comprise multiple functional subtypes, each of which independently tiles the retina. We provide evidence for the latter, illustrating that like conventional RGCs, ipRGCs are arranged in mosaics optimal for the even representation of visual space. But the retinal distribution of ipRGCs and how this relates to specific subtypes of M1 ipRGCs has remained elusive.

Here we provide the first evidence that like conventional RGCs, ipRGCs are arranged in a tiled mosaic optimal for the even representation of visual space. We use a combination of mouse genetics, confocal microscopy, anterograde and retrograde labelling, patch clamp recordings and optogenetics to describe a subtype of M1 ipRGCs that are found only in the peripheral dorsal retina. They form a regularly spaced mosaic within this region suggesting mice devote additional melanopsin-dependent processing power to their ventral visual field. This subtype of M1 ipRGCs forms the primary visual projection to the SON, and project to unique sub-regions of other non-image forming brain nuclei, like the SCN and IGL, where they release the excitatory neurotransmitter glutamate, despite having *Cre* expression driven by the promotor of the glycine transporter GlyT2.

Results

A unique population of ipRGCs encoding ventral vision

We discovered RGCs in mice where *Cre* is driven by a BAC encoding the inhibitory glycine transporter GlyT2 (slc6a5 KF109;[30] Fig. 1a). In these mice, *Cre* is expressed both in GABAergic and glycinergic neurons in the retina and brain[31]. In retina, Cre expression is overwhelmingly restricted to inhibitory amacrine cells such as the glycinergic AII amacrine cell [32]. However, we also observed fluorescent axons in the ganglion cell layer (Fig. 1a), and when following them to the optic nerve head discovered they originated

solely from RGCs in the dorsal retina (Fig. 1c). Hypothesizing these RGCs likely represent a unique feature selective population in the retina, we sought to determine their functional identity by mapping their central axonal projections in the brain with *Cre*-dependent anterograde labelling of their axon terminals and their light responses and dendritic morphology with targeted electrophysiological recordings and Neurobiotin fills.

To determine the location of the central projections of their axon terminals, we injected an AAV into the eye enabling the *Cre*-dependent expression of fluorescent protein (Fig. 1b). The axons of RGCs labeled using this method predominantly innervated non-image forming brain regions such as the intergeniculate leaflet (IGL) and suprachiasmatic nucleus or nuclei (SCN) (Fig. 1d), suggesting they arose from ipRGCs, which form the predominant projections to these regions. To confirm their identity in the retina, we performed melanopsin antibody co-staining in *GlyT2^{Cre};Ai140* mice (Fig. 1e) and *GlyT2^{Cre};Ai9* mice (Fig. S1) and found that fluorescent RGCs in the dorsal retina co-expressed melanopsin. We subsequently targeted fluorescent cell bodies in isolated preparations of dorsal retina from *GlyT2^{Cre};Ai9* mice for electrophysiological spike recordings. Current clamp recordings from fluorescent somas allowed us to confirm intrinsically photosensitive spike responses in the presence of a cocktail of excitatory synaptic blockers (Fig. 1f; 20 µM L-AP4, 25 µM DAP5, 20 µM CNQX).

To identify the dendritic morphology of these ipRGCs, we performed cell targeted Neurobiotin fills in the RGC layer of *GlyT2^{Cre};*Ai9 retina. These experiments revealed they are predominantly comprised of an OFF stratifying type, a structural feature of M1 ipRGCs [33,34] (Fig. 2a). We also found they contained a secondary population stratifying in the ON layer, with variable morphologies, resembling a mixture of non-M1 ipRGCs[35-38]. Characterizing their dendritic structure using Sholl analysis (Fig. 2b), we found that the morphological complexity of the OFF stratifying cells, including the total number of branching points, junctions, and end-points are distinct from the mixture of ON stratifying cells (Fig. 2b,c). Furthermore, the soma diameter (Fig. 2d), dendritic diameter (Fig. 2e), and pattern of Sholl crossings (Fig. 2b) measured in the OFF stratifying cells are consistent with previous studies of M1 type morphology.

To determine the spatial location of *GlyT2^{Cre}*-positive ipRGCs, we generated distribution maps in wholemount preparations of *GlyT2^{Cre};Ai140* retina using melanopsin antibody co-staining and confocal microscopy. *GlyT2^{Cre}*-expressing cells (Fig. 3a,b), and melanopsin expressing ipRGCs (Fig. 3c,d) were found across the entire retina (Fig. 3b,d). However, GFP-positive ipRGCs (Fig. 3e) were localized to the dorsal periphery of the retina (Fig. 3f), interspersed among other dorsal ipRGCs (Fig. 3e). Their location in the dorsal retina resembles the asymmetric distribution of cone photoreceptors, more specifically the region of retina that contains predominately green cones and few UV cones[39,40]. Co-staining with the mouse s-opsin antibody that selectively labels UV opsin we show that *GlyT2^{Cre}*-positive expressing ipRGCs are located above the UV cone transition zone (Fig. 3g,h), occupying the dorsal region of retina with low UV cone density (Fig. 3f,h,g).

Previous studies report that M1 ipRGCs are denser in the dorsal retina[3,41-43], so we reasoned that GlyT2^{Cre}-expressing M1 ipRGCs might be a unique subtype that accounts for the asymmetry. If our hypothesis is correct, the density of M1 ipRGCs in the dorsal and ventral retinas should be the same if we discount the *GlyT2^{Cre}*-positive M1 ipRGCs. To test this hypothesis we examined the retinal distribution of all M1 ipRGCs using confocal microscopy. M1 ipRGCs have sparse dendritic arbors stratifying in the OFF IPL (Fig. 4a) and express the highest amount of melanopsin[29,34], making them easier to identify using immunohistochemistry and confocal microscopy. Whole retina density maps of M1 ipRGCs (n ≈ 800 cells) confirm their increased dorsal density (Fig. 4b)[42] and they were evenly interspersed with *GlyT2^{Cre}* M1 ipRGCs (Fig. 4c, n ≈ 150 cells). When we subtracted *GlyT2^{Cre}*-positive ipRGCs (Fig. 4d-g), the density of M1 ipRGCs between the dorsal and ventral retina were equivalent, confirming our hypothesis (Fig 4i, j). These results suggest the mouse visual system dedicates an additional M1 ipRGC visual channel to the ventral visual field. We reasoned this anatomical segregation in the retina might be mirrored in their central axonal projections, which are segregated in previously identified subtypes of M1 ipRGCs. These distinct separations of ipRGC central projections underlie distinct behavioral functions[10,16,18].

GlyT2^{Cre} ipRGCs innervate the outer core of the SCN

To determine the central axon projection sites of GlyT2^{Cre}-positive ipRGCs we performed intravitreal eye injections of *Cre*-dependent AAV (Fig 1, Fig. S2). Cholera toxin B (CTB), was later injected to co-label retinorecipient axon terminals (Fig. S2). To provide anatomical reference, these regions were also compared with the CTB labeled projections of all RGCs (Fig. S5a,d,g,j) and eye injections performed in the *OPN4*^{Cre} transgenic mouse, a line which labels all ipRGCs (Fig. S5c,f,l,l). Summary central projection traces were also generated for the GlyT2^{Cre} ipRGCs (Fig. S6). Like many other ipRGCs, *GlyT2*^{Cre}-positive ipRGCs project to the SCN, but this projection is unique for several reasons. First, their axonal projections to the SCN avoid a central core region (Fig. 5a), and are concentrated at the ventral and lateral regions (Fig. 5a,b,d). Serial sections through the SCN in *GlyT2*^{Cre};Ai32 mice, which express CHR2-eyfp in the axon terminals of the GlyT2^{Cre}-positive ipRGCs, illustrate that their axons did not project to the classically defined shell of the SCN (Fig. 5 c,e & Fig. S3), which is delineated by the anatomical localization of neurons that express arginine vasopressin (AVP) [44-49]. Rather, they project to a subregion of the classical core, which we refer to as the *outer core* as their axons avoid AVP neurons (Fig 5c,d,e,i). In the anterior SCN, their axon terminals were located ventrally (Fig. 5i & Fig. S3a) in a region associated with neurons expressing vasoactive intestinal peptide[44]. In more caudal regions their axons formed a peripheral shell around the SCN core, and were densest in the ventral and lateral regions (Fig. 5c, l & Fig. S3b,c). At the most caudal region of the SCN, their axon terminals formed a *lateral band* with excursions outside of the SCN into the anterior hypothalamus and lateroanterior hypothalamus (Fig. 5d,e,i & Fig. S3d). The projections suggest that *GlyT2*^{Cre}-positive ipRGCs likely contribute to distinct functional light-entrainment of circadian rhythms. The functional role of their projections to the AHC and LA outside of the SCN remain unclear however these regions are thought to be involved in thermoregulation [50] and aggression control[51-53].

Outside of the SCN the GlyT2^{Cre} positive ipRGCs innervated the SON, which contains neurons expressing AVP and oxytocin (Fig. 5d-i) and is thought to be involved in systemic fluid homeostasis[54], parturition[55], and appetite[56,57]. It is also thought that the innervation

of this region is exclusively from Brn3b+ M1 ipRGCs[4,6,16]. *GlyT2^{Cre}*-positive ipRGC axons most prominently innervated the region of the SON immediately dorsal to the optic tract and dorsomedial to the SON known as the perinuclear zone (Fig. 5d; pSON) [4,16,58]. Some of their axons did however, innervate the SON in addition to extending medially into the lateral hypothalamus (Fig. 5f-h,j & Fig. S4a). Outside of the hypothalamus, their axons formed prominent projections to the zona incerta (Fig. S4b)[4], IGL and parvocellular division of the vLGN (Fig. S5b), the lateral posterior nucleus (Fig. S5b), the ventral shell of the OPN (Fig. S4b,d,e - blue) and pretectal regions ventral to the superior colliculus (Fig. S5d,e,g,h,j,k). Many of these *GlyT2^{Cre}* ipRGC projections, particularly the SON, accessory hypothalamic nuclei, and the OPN shell are regions thought to be innervated primarily by M1 ipRGCs[6].

SON-ipRGCs: a mosaic of ipRGCs retro-labeled from the SON

Due to the heavy innervation of the pSON and surrounding areas when compared with previous reports, we hypothesized that (1) *GlyT2^{Cre}*-positive ipRGCs may be the sole projection to this region, and (2) that only the M1 morphological type of GlyT2^{Cre}-positive ipRGCs project to this region[15,59]. Since it is comparatively isolated from the SCN and the LGN, we decided to selectively target M1 *GlyT2^{Cre}*-positive ipRGCs using retrograde injections of Cre-dependent AAV injected into the pSON (Fig. 6a,b). These injections labeled melanopsin positive M1 ipRGCs in the retina with dendrites in the OFF layer which restricted to the dorsal hemisphere and in similar density to those identified in *GlyT2^{Cre};Ai140* (Fig. 6c,f,g; 113 ± 5.4; n = 2 mice). Next, we performed the same injections in OPN4^{Cre} mice, which expresses Cre in all ipRGCs, to determine if the dorsal location and OFF stratification of these SON-labeled ipRGCs is specific to neurons expressing *GlyT2^{Cre}* (Fig. 6d-g). Significantly, the majority of ipRGCs labeled with these injections were OFF-stratifying M1 ipRGCs (~97%) (Fig. 6d,e,f) and located in the dorsal retina in similar quantity and distribution to those labeled in *GlyT2^{Cre}* mice (n = 131 ± 16.4 OFF ipRGCs, n = 4 ± 1 ON ipRGCs, n = 3 animals) and similar in number to those quantified from our counts of GFP and melanopsin positive M1 ipRGCs in *GlyT2^{Cre};Ai140* mice (Fig. 6f & Fig. 4).

We observed a small number of ventral OFF ipRGCs labeled by AAV injections into the SON in OPN4^{Cre} mice, in addition to a small number of ON ipRGCs (Fig. 6d,f; n = 27 ± 5.5 ipRGCs). As these ipRGCs were (1) rarely labeled, (2) restricted to small regions, and (3) the ON ipRGCs were also predominantly in the ventral retina, we conclude that this is most likely due to spillover of AAV into the optic tract which lies immediately ventral to the SON. We also noticed some non-ipRGCs, which appeared to be amacrine cells labeled in the retina (*GlyT2^{Cre}* 2 ± SD 2.6 neurons from 3 mice; *OPN4^{Cre}* 5.3 ± SD 5 neurons from 3 mice). We conclude that their labeling likely arose from trans-synaptic labelling, or viral spillover from ipRGCs in the retina, as they do not have axons passing out of the retina. Together these data suggest that the dorsal GlyT2^{Cre} ipRGCs represent the sole retinorecipient projection to the SON, and further strengthens our conclusions from anatomical mapping data illustrating these ipRGCs represent a distinct subtype that is located solely in the dorsal retina. Because these ipRGCs represent the exclusive projection to the SON, we now refer to them as SON-ipRGCs.

We noticed that SON-ipRGCs were evenly spaced in our anatomical mapping experiments and uniform mosaic distribution of RGCs is one of the defining characteristics of a unique functional subtype. Our retro-labelling of SON ipRGCs with brain injections into *GlyT2^{Cre}* and *OPN4^{Cre}* mice was even more striking. The dendrites of SON-ipRGCs in the dorsal retina formed non-overlapping territorial mosaics, reminiscent of other territorial RGC subtypes (Fig. 7a-c)[24,25]. Upon close examination using confocal microscopy, the dendrites of SON-ipRGCs overlapped with the dendrites of other OFF stratifying ipRGCs in sublamina-a of the IPL stained with anti-melanopsin, and displaced M1 ipRGCs somata (Fig. 7d). SON ipRGCs have a uniform and unique dendritic morphology with 3-4 short dendritic segments that project through the ON layer and extend their terminal dendrites in the OFF layer (Fig. 7e,f). To provide a quantitative framework of analysis of the mosaic distribution of SON ipRGCs, we quantified (1) the density recovery profile[60,61], a measurement of cell density at increasing distances from the soma (Fig. 7g & Fig. S7a,b,d), and (2) the coverage factor, which is a quantitative measurement of dendritic overlap in mosaic distributions (Fig. 7h & Fig. S7c). Our density

recovery profile data indicated that M1 ipRGCs and non-SON projecting M1 ipRGCs together overlapped significantly as evidenced by high values in very close proximity to the soma (< 100 µm) (Fig. 7g). SON-ipRGCs labeled with retro-injections in *GlyT2*^{Cre} and *OPN4*^{Cre} mice exhibited a clearly defined exclusion zone around the soma, which indicates their cell bodies are regularly spaced (Fig. 7g, Fig. S7). We next examined their coverage factor, which measures the average number of dendritic fields within a RGC mosaic overlapping any point in space. Most RGC subtypes that represent a functional visual channel have a coverage factor ~2 indicating there are roughly 2 dendritic fields (or receptive fields) of each specific functional visual channel at any point in the retina[62]. To calculate the coverage we used the average dendritic field diameter from morphological Neurobiotin fills (324 ± 18 µm), as the edges of the dendritic fields labeled from SON virus injections were difficult to resolve due to their overlap. Using these measurements we found that SON-ipRGCs had a coverage factor of just over 2 (2.2 ± 0.18 *GlyT2*^{Cre}; 2.1 ± 0.03 *OPN4*^{Cre}) indicating each point in the dorsal retina is covered by at least 2 ipRGCs. Non SON-projecting ipRGCs has a coverage of 3.6 ± 0.19, and all M1 ipRGCs has a coverage factor of 5.7 ± 0.16 (Fig. 7h & Fig. S7c & Supplementary table 2). This indicates that SON ipRGCs are territorial, and provide a seamless coverage of the retina with minimal overlap, similar to some other highly territorial RGC subtypes[25]. These results also support the hypothesis that there are two more territorial M1 ipRGCs subtypes in the dorsal retina or an additional subtype of M1 ipRGCs with higher coverage and slightly more overlap with SON-ipRGCs. Together, these results strongly support the hypothesis that there are multiple ipRGC subtypes in the dorsal retina and that SON-ipRGCs are a unique subtype.

Next, we examined other central projection locations following SON injections (Fig. S8). As these mice only have OFF stratifying SON-ipRGCs labeled in the retinas, this allows us to determine the projection patterns without contamination from other ON stratifying ipRGCs that are labeled using anterograde injections into the eye (Fig. 5,S2, & S4). These results illustrate that the unique projections to the *outer core* of the SCN are from SON-ipRGCs (Fig. S8d,e) and patterns of innervation appeared similar between *GlyT2*^{Cre} and *OPN4*^{Cre} animals. Projections to the IGL, a site of accessary circadian function, was also

observed (Fig. S8f,g). These results suggest that the IGL, SON and *outer core* of the SCN are co-innervated by a single dorsal subtype of ipRGCs, the SON-ipRGCs.

SON-ipRGCs release glutamate at central synapses

Having established that SON-ipRGCs represent a unique subtype of M1 ipRGCs according to their expression and distribution in the retina, we asked if their targeting in *GlyT2*^{Cre} mice underlies unique neurotransmitter release in the brain. This is particularly important given the recent discovery that some ipRGCs, which project to the SCN, IGL, and OPN release GABA at their central synapses[63]. As SON-ipRGCs are labeled in a mouse line that selectively labels inhibitory neurons throughout the brain and retina, we asked if they released GABA or glycine using two optogenetic approaches to express channelrhodopsin in their axon terminals and to record light-evoked neurotransmitter release (Fig. 8 & Fig. 9). We chose to record from multiple central locations to rule out the possibility SON-ipRGCs differentially release neurotransmitters at different central locations. Our recordings were focused primarily in the SCN and IGL, due to their dense innervation from SON-ipRGCs, but we also recorded from the SON to test for direct synaptic connectivity between the retina and the SON.

We crossed GlyT2^{Cre} mice with a Cre-dependent ChR2^{EYFP} reporter (Ai32; Jackson 024109), which results in the expression of ChR2 in the axons and nerve terminals of SON-ipRGCs (Fig. 8a-e). Lateral SCN neurons were targeted in coronal slices (Fig. 8b). In cell-attached voltage clamp mode photo-stimulation activated robust action potential currents (APC), which demonstrates that the SCN neuron was depolarized beyond its action-potential threshold by the release of an excitatory transmitter. The amplitude and latency of APCs (Fig. 8h) were robust and fast, consistent with monosynaptic excitatory synaptic connections (Fig. 8g; (mean ± SEM) 7.2 ± 0.5 ms (range 6.3 – 8.2 ms) and 193.7 ± 74.2 pA (range 53.8 – 306.3 pA), n = 3). In whole cell voltage clamp recordings we detected photo-stimulation evoked inward post-synaptic currents (PSCs) at holding potentials between -60 mV and -40 mV (Fig. 8f). The PSCs latency and amplitude were 6.7 ± 0.2 ms (range 6.3 – 7.4 ms) and 35.2 ± 10.0 pA (range 15.4 – 71.3 pA), n = 5, Fig. 8g, h. Similar excitatory synaptic input to SCN neurons was demonstrated by electrical

stimulation of the optic chiasm (Fig. 8b,f-h) which resulted in larger and faster PSCs (Fig. 8 f,h). Pharmacological blockers were used to identify the neurotransmitter released by SON-ipRGCs. The glycine receptor antagonist strychnine (1 µM) and the $GABA_A$ antagonist SR-95531 failed to inhibit photo-stimulation-induced PSCs (Fig. 8f,i). In contrast, PSCs were blocked by co-application of the selective AMPA and NMDA glutamate receptor antagonists CNQX (20 µM) and AP-5 (50 µM) (Fig. 8f,i,j). Similarly, in cell-attached mode, photo-stimulation-induced APCs were inhibited by co-application of CNQX and AP-5 (Fig. 8j). Together, these results are consistent with a model where SON-ipRGCs are excitatory and release glutamate onto SCN neurons.

The whole-cell patch electrodes contained Neurobiotin and the location of recorded SCN neurons and their proximity to SON-ipRGC axon terminals was reconstructed with confocal microscopy. While only a small percentage of recordings resulted in photo-stimulation evoked PSCs, the locations of connected neurons were mapped to each slice by referencing infrared microscopy images taken of the living slice with the subsequent post-fixed confocal images (Fig. 8k). The locations of synaptically connected SCN neurons were consistent with anterograde and retrograde tracing experiments showing SON-ipRGC axon terminals resided in the *outer core* of the SCN (Fig. 5 & Fig. S3). Similar inward PSCs with a latency of 5.72 ± 0.13 ms (range 5.56 – 5.98 ms, n = 3) and amplitude of 64.7 ± 7.1 pA (range 55.9 – 78.9 pA, n = 3) which were not blocked by picrotoxin (50 µM) were recorded in voltage clamped SON neurons (Fig 8 i-o). Electric stimulation of the optic chiasm evoked PSCs in SON neurons confirming the retinal projection to this nucleus (latency 2.6 ± 0.2 ms, amplitude 215.8 ± 50.1 pA, n = 6).

To determine if SON-ipRGCs might differentially release neurotransmitter at separate central locations, we performed whole-cell voltage-clamp recordings in the IGL in coronal slices made from *GlyT2^{Cre};Ai32* mice (Fig. 9a, b). To enhance chloride-mediated currents high chloride (65 mM CsCl-) internal solution was used, which changed the inhibitory reversal potential to -50 mV and allowed us to observe inward PSCs for both excitatory and inhibitory events. Photo-stimulation in the IGL resulted in mixed neurotransmitter release, with evidence for GABA, glycine, and glutamate release in our recordings (Fig.

9 c-g). Most photostimulation-evoked synaptic currents were stable in the presence of CNQX, and were strongly attenuated by strychnine, and completely abolished in a combination of CNQX, strychnine, and GABAzine (Fig. 9e-g). These results were seemingly in conflict with our SCN recordings and might suggest that SON-ipRGCs release inhibitory neurotransmitters in the IGL while releasing excitatory neurotransmitters in the SCN. However, the IGL receives inhibitory input from other central brain regions[64], some of which may contain neurons labeled in the *GlyT2^{Cre}* mouse line and may express ChR2 on the cell membrane in *GlyT2^{Cre};Ai32* mice.

To determine whether photo-stimulation-evoked inhibitory PSCs in the IGL arise from non-retinal neurons, we restricted ChR2-expression to the retina with eye injections of Cre-dependent ChR2 in *GlyT2^{Cre}* mice (Fig. 9h). After allowing 2 – 3 weeks for the ChR2 to express, we recorded from the IGL, which was targeted in coronal slices with brief epi-fluorescent illumination to identify eGFP-expressing axon terminals, which form a dense band in the IGL (Fig. 19i - green). IGL neurons were filled with biocytin and recovered for confocal microscopy (Fig. 9j). Photo-stimulation evoked inward PSCs that were completely abolished with the bath application of the AMPAR antagonists CNQX and NBQX (Fig. 9k). These excitatory PSCs were on average smaller than evoked in recordings from *GlyT2^{Cre};Ai32$^{ChR2:EYFP}$* mice, which may be due to viral expression of ChR2 being lower than expression driven by the *Ai32* line. To augment photostimulation-induced PSCs and rule out the possibility that inhibitory synaptic terminals need greater depolarization to reach the threshold required to activate transmitter release, we included K-channel blocker 4-aminopyridine (4-AP) in the ACSF and also included tetrodotoxin (TTX) to abolish poly-synaptic events. Despite 4-AP substantially increasing the light-evoked currents they were completely abolished by the co-application of CNQX (Fig. 9k). Thus, when ChR2 was expressed in the axon terminals of ipRGCs of *GlyT2^{Cre}* or *OPN4^{Cre}* mice, no evidence for inhibitory synaptic release was found. This suggests that inhibitory inputs to the IGL in *GlyT2^{Cre};Ai32* mice likely arise from central regions where neurons expressed ChR2 activated by light, and that SON-ipRGCs only release glutamate, but not GABA or glycine.

Discussion

Mosaic tiling and distribution

In most retinal ganglion cell subtypes the fundamental organizing feature of retinal output is a mosaic, where the receptive field and corresponding dendritic fields of individual cells of the same subtype are arranged in territorial, regularly spaced grids[43,65,66]. Such arrangement leads to uniform coding of the visual scene across each retinal channel. This has remained unclear for ipRGCs, which overlap considerably, about 4-fold in the retina for the M1 ipRGCs[29]. As M1 ipRGCs participate primarily in non-image forming vision it is possible that spatial organization is deemphasized in favor of maximizing the area of photon capture[67]. Our results show that M1 ipRGCs can be further subdivided and comprise independent subtypes that tile retinal space, like many of the well-described conventional *bona fide* RGC subtypes[25,66,68,69]. Indeed the coverage factor of SON-ipRGCs is similar to the average coverage factor of most RGCs, identified from their functional receptive fields[62]. This indicates SON-ipRGCs are territorial and their dendrites overlap minimally. The functional significance of this arrangement is unclear, but it suggests surprisingly, that retinotopy might also be important for circadian biology[70], and other non-image forming functions mediated by the SON.

Our mapping data illustrates that the increased density of ipRGCs in the dorsal retina[3,41] arises from an additional population of ipRGCs found only in this region. There are two pieces of evidence supporting this conclusion; (1) when SON-ipRGCs are subtracted from retinal density maps, the dorso-ventral density gradient disappears and the number of M1 ipRGCs is equivalent in both hemispheres. (2) Retrograde labelling of SON-ipRGCs in OPN4Cre mice labels the same dorsal M1 ipRGCs as those localized in the GlyT2Cre mouse. These results suggest that there are at least 2 independent populations of M1 ipRGCs in the dorsal retina, each with their own appropriate coverage factors. We estimate that SON-ipRGCs overlap ~twice, whereas the total population of M1 ipRGCs in the dorsal retina overlap ~5.5-fold. These values were calculated using the average dendritic diameter of Neurobiotin filled M1 ipRGCs in the *GlyT2Cre* mouse (d = 324 µm)

and are slightly larger than the dendritic diameter of M1 ipRGCs previously described (d = 274 μm)[29], resulting in slightly different coverage values (Fig. S7c). Though these differences are likely due to labeling technique, we cannot exclude the possibility that SON-ipRGCs have a different dendritic structure than neighboring M1 non-SON-ipRGCs). Currently it remains unclear if the ventral M1 ipRGCs belong to the same subtype of ipRGCs as those in the dorsal retina that overlap with the SON-ipRGCs. If the overlapping M1 ipRGCs follow the same spacing and distributions as the SON-ipRGCs, then there are at least two distinct subtypes of M1 ipRGCs in the rodent retina; one that is distributed across the entire retina and one that tiles the dorsal retina.

Localized vision and photoreceptor organization

The dorsal-only location of SON-ipRGCs suggests retinotopy at the level of the dorso-ventral axis is fundamental for some types of non-image forming vision. For the rodent, the horizon divides the visual scene into two distinct areas, consisting of differences in color, contrast, and behavioral relevance[39]. Accordingly, this is reflected in the asymmetric organization of cone photoreceptors across the dorso-ventral axis of rodent retina[39,40]. The higher density of UV-sensitive cones in the ventral retina enhances the dynamic range of photoreceptors for encoding the darker contrasts, which dominate the upper visual field and is likely important for predator detection[39,43]. Similarly, the dynamic range of the green cones that are in abundance in the dorsal retina is matched to encode the more even distribution of both light and dark contrasts found in the ventral visual field, likely aiding in navigation through foliage or burrows and finding small grains, grass and insects for consumption.

While rodent RGCs can form non-uniform topographic variations across the retina[71], SON-ipRGCs are the first example of a RGC subtype restricted to a sub-region of retina. Strikingly, their location is almost identical to the region of dorsal retina that is low in UV-sensitive cones, suggesting ipRGCs and cone photoreceptors may have adapted similarly to encode information that is asymmetrically distributed in visual space. Non-image forming vision might also be adapted to encode the more uniform distribution of bright and dark contrasts, like cone photoreceptors. Alternatively, as the visual system of

the rodent is optimized for nocturnal vision, they might require additional processing power in night or daylight environment. Moon and starlight reflected off the ground is likely to predominate in nocturnal environments and reflected luminance might contain more useful information to drive the suppression of SON-mediated behaviors such as maternal activity or feeding[72,73].

Central projections and behavioral relevance

There are currently six known types of ipRGCs (M1–M6), primarily distinguished by their morphology[6,12]. However, recent evidence suggests additional functional subtypes likely exist within this current organization[10,16,18,22,36,63,74]. How do these additional ipRGC subtypes fit with our current understanding of M1 ipRGCs? Some ipRGCs do not express the transcription factor Brn3b and this small number of ipRGCs projects to the SCN and IGL only, avoiding other brain regions[18]. Our results suggest that a separate tiling subpopulation of M1 ipRGCs co-innervate the SON, the outer core of the SCN and the IGL, likely performing distinct behavioral functions.

The SON is a collection of secretory cells that participate in the hypothalamic-pituitary-adrenal axis by producing antidiuretic hormone (ADH) and oxytocin. ADH is responsible for regulating water reabsorption in the kidneys[75] and oxytocin plays a critical role in lactation and parturition[76]. The significance of visual input to this area via the SON-ipRGCs is unclear but circadian changes in urine volume and concentration[77,78], as well as patterns of lactation[79,80] are well established in humans and animal models. Like the influence of ipRGCs on entrainment of the SCN, bright light might act as a Zeitgeber in the SON, keeping the daily release of AVP well-timed or to aid in adjusting fluid balance to altered light cycles, such as when changing time zones. Alternatively, ipRGCs that innervate the SON might be involved in more direct effects of light on the release of AVP or oxytocin by SON neurons. It is also possible that SON-ipRGCs regulate the release of oxytocin, AVP, or other neuropeptides such as cholecystokinin, or CART, throughout the brain, rather than in the pituitary, where SON ipRGCs might be important for regulating direct light-activated influence on maternal behaviors, or feeding[81]. Future studies of sex differences in these pathways will be interesting in this regard.

Separate ipRGC populations influence both the circadian and direct effect of light on body temperature[10]. It is possible that innervation to the SON functions similarly, acting as a synchronizer of different SON-mediated behaviors over shorter timescales than those governed by the SCN. The peptide pituitary adenylate cyclase-activating polypeptide (PACAP) is present in a dorsal population of ipRGCs in the rat[41] and both PACAP and the PACAP receptor PAC_1 are expressed in the SON[82,83]. Additionally, PACAP positive retinal hypothalamic tract terminals are localized to a SCN region that resembles the outer-core projections of SON ipRGCs. Thus SON ipRGCs are likely the PACAP-containing ipRGCs described in rat retina but further studies are required to specifically determine this.

The unique innervation of SON-ipRGCs to known circadian structures (SCN and IGL) is also of significant interest. Oscillatory activity in the SCN functions as a circadian timing circuit, predicting physiological and behavioral needs throughout the day and night[84]. The SCN is divided into two distinct subdivisions, designated as core and shell based primarily on localized peptidergic expression, innervation, and projection[85]. The core is the site of direct visual input from ipRGCs, indirect visual input from IGL, and is localized by the expression of vasoactive intestinal polypeptide (VIP) and gastrin releasing peptide (GRP)[44]. Alternatively, the SCN shell contains a large number of AVP neurons and receives innervation from other CNS nuclei[44,86]. Our results show that SON-ipRGCs innervate a localized region of the SCN we call the outer core, avoiding the central core of primary ipRGC input and the AVP neurons that comprise the SCN shell. As SON-ipRGCs represent a distinct subtype of ipRGC it suggests that the SCN receives at least two types of direct retinal input, segregated to at least two localized areas of the SCN. The behavioral relevance of this organization is unclear but given the localized distribution of SON-ipRGCs in the retina, and their overlap with other M1 ipRGCs, it suggests that subtypes may be encoding different aspects of environmental light. Given their broad projections to the SCN, IGL, SON and other regions, and the limited knowledge of their specific connectivity within the SON, behavioral analysis of the specific functional role of

this unique subtype would require surveying many behaviors that might rely on subtle inputs from SON-ipRGCs.

Neurotransmitter release

Why are there ipRGCs labeled in the *GlyT2*^{Cre} line, which, other than ipRGCs, labels predominantly glycinergic amacrine cells in the retina? This question is particularly prescient given the recent discovery of GABAergic ipRGCs that project to the SCN, IGL and OPN[63]. Our results, however, indicate that SON-ipRGCs do not release GABA, and thus must form a separate population from GABAergic ipRGCs. It remains unclear if they express the *GlyT2* transporter in their axon terminals, and if they do, what functional role the transporter might play in modulating central synapses. It is possible that SON-ipRGCs release glycine to modulate the glycine binding site on post-synaptic NMDA receptors however there is no evidence of synaptic release of glycine in the SCN because spontaneous glycinergic IPSCs were not present and glycine does not contribute to the tonic current as strychnine did not alter the baseline of SCN neurons[87]. Alternatively their labelling in *GlyT2*^{Cre} mice may be some other function of the bacterial artificial chromosome (BAC) insertion in this particular transgenic line. Indeed, other BAC lines, like the *HB9*^{GFP} line that labels ON-OFF direction selective ganglion cells, reflect the genomic insertion site of the BAC[88].The BAC maps to chromosome 12 rather than the endogenous location of chromosome 7. Regardless, our anatomical mapping data predicts there are likely only two subtypes of ipRGCs in the dorsal retina, if other ipRGCs follow similar mosaic spacing rules as SON-ipRGCs. While we do not know if GABAergic ipRGCs are M1 ipRGCs, their projections to the SCN strongly suggest some of them are, whereas their projections to the shell of the LGN might indicate some are not ipRGCs[63]. Given they are more numerous in the dorsal retina, it remains unclear if they are the other subtype we predict to lie in the dorsal retina or, instead, they might be part of multiple subtypes of ipRGCs that do not form complete mosaics throughout the retina. Future studies of both retrograde tracing of these populations and functional recording from ipRGCs in the retina and brain are required to resolve these questions.

Methods

536 **Animals**

537 Experiments involving animals were in accordance with the National Institutes of Health
538 guidelines, and all procedures were approved by the Oregon Health and Science
539 University Institutional Animal Care and Use Committee. *GlyT2*^{Cre} mice (Tg(Slc6a5-
540 cre)KF109Gsat/Mmucd) were a gift from Larry Trussell, prior to being cryo-recovered by
541 the OHSU Transgenic Mouse Model Core using sperm purchased from the Mutant Mouse
542 Resource and Research Center (Stock 030730-UCD). Ai32 (RCL-ChR2(H134R)/EYFP),
543 Ai9 (RCL-tdT), and *Ai140* (TITL-GCF-ICL-tTA2) mice were obtained from The Jackson
544 Laboratories. *OPN4*^{Cre} (tm1.1(cre)Saha/J) were a gift from Samer Hattar and The Johns
545 Hopkins University. Animals were bread and housed on a 12-h light/dark cycle with food
546 and water ad libitum.

547

548 **Eye and brain injections**

549 To trace ipRGC projections and sites of central innervation, anterograde tracers were
550 delivered in the eye through intravitreal injection. AAV-FLEX-tdTomato (Catalog# 28306
551 AAV2 & PHPeB; 2 µl per eye at 1×10^{13} vg mL^{-1}) and AAV1-DF-ChR2-mcherry (Catalog#
552 18916) were purchased through Addgene. For this procedure, animals were anesthetized
553 by intraperitoneal injection of 100mg/kg ketamine, 15mg/kg xylazine. Proparacaine
554 (anesthetic) and tropicamide (anticholinergic) drops were applied topically to the eye for
555 local anesthesia and to improve visualization of the surgical field, respectively. Under
556 stereo microscopic control, a small hole was made at the ora serrata using a 32G needle.
557 AAV vectors containing ~10^{13}-10^{14} viral genomes were delivered in 1.5 µL volumes to the
558 vitreous of the eye using a 5 µL Hamilton microinjection syringe. Animals were allowed to
559 recover from anesthetic on a heat pad before being returned to their cage. AAV injections
560 were performed between p30–p60. To aid in visualizing retino-recipient brain structures
561 animals also received a follow up eye injection of 1uL CTB-488 one week before sacrifice.
562 In order to identify ipRGCs that innervate specific central locations, stereotactic brain
563 injections of retrograde tracers were performed using a Kopf stereotactic instrument. For
564 the supraoptic nucleus (SON), 92nL of AAVRG-DF-ChR2-mcherry (Catalog# 18916) was
565 injected bisymmetrically at 0.5mm from Bregma, +1.3mm lateral to the midline at a depth

of 5.0mm, determined from the Franklin & Paxinos Mouse Brain Coordinate Atlas, 4th ed. Animals were sacrificed three-four weeks following injections for brain and eye histology.

Tissue preparation and immunohistochemistry

For retina histology, animals were euthanized with 200mg/kg ketamine and 30mg/kg xylazine followed by cervical dislocation. Eyes were then removed with curved surgical scissors and placed in 4% paraformaldehyde (PFA) (Electron Microscopy Sciences Catalog#: IC993M31) in phosphate buffered saline (PBS) for 30 mins with the cornea partially removed. Eyes were then washed thoroughly in PBS for 24hrs. To dissect the retina from the eye, the lens and tissue up to the trabecular meshwork was removed leaving an exposed globe. Dorsal ventral orientation, marked with a ventral cut, was established using the choroid fissures and retinal artery, which can be visualized entering the caudal portion of the sclera, inferior to the optic nerve. The retina was then separated from the sclera by cutting along the rim of retinal attachment and transecting the optic nerve from its scleral bed. Whole retina was then transferred to a 1.5ml Eppendorf tube for immunohistochemistry. The details, including the timing and concentration of primary and secondary antibody used for specific experiments are described in Table 1. Once immunostaining was complete, 3 additional relieving cuts were made at cardinal positions to allow the whole retina to be flat-mounted RGC side up on glass slides. Retinas were dried on the slide until transparent, then mounted with a coverslip using Vectashield mounting medium.

For brain histology, animals were heavily anesthetized by IP injection of ketamine/xylazine and transcardially perfused with 50µL Heparin + 30 mL PBS followed by 40mL 4% PFA in PBS. Brains were removed and post-fixed in 4% PFA 2-4 hrs. Brains were then washed thoroughly in PBS for 24hrs, mounted in 4% agar and sectioned at 200µm from rostral to caudal using a Leica VT1000 S vibratome. Sections were collected in PBS and transferred to glass slides. Retinas and brain slices were immuno-stained in a mixture of 5% Donkey serum, 0.5% Triton-X 100 and 0.25 % sodium azide at room temperature. Details, including the timing and concentration of primary and secondary antibodies used for specific experiments are described in Table 1. Both brain slice and

whole-mount retina were mounted using Vectashield mounting medium (Vector laboratories) and imaged on a Leica SP8 scanning confocal microscope.

Quantification of retina histology

To generate retina maps, whole retina tiling confocal z-stacks were captured using Leica SP8 confocal microscope using a 40x oil objective. Tiles were stitched together in Leica LAS X Life Sciences software and analyzed in ImageJ. ipRGCs were manually identified across the entire retina by systematically localizing all melanopsin positive cell bodies in 200 x 200 µm square increments. Somas were marked as regions of interest (ROI) in a separate overlay image using the multipoint tool in imageJ (2d axis image). M1 ipRGCs were identified by their characteristic dendritic stratification in the OFF sublamina, their small somas, and bright melanopsin staining. *GlyT2^{Cre}* ipRGCs were identified by the co-localization of GFP and melanopsin in their cell bodies (*GlyT2^{Cre};Ai140*). Distribution maps of ipRGCs were generated from the x/y coordinates extracted from the axis image. Due to their abundance, UV cone distribution maps were generated using the trainable Weka segmentation plugin for imageJ [89] (imagej.net/plugins/tws/). This machine learning software allows structures of similar appearance to be identified in a semi-automated manner. Images were processed with a binary threshold and segmentation was trained to identify fluorescent cells (UV+ cone outer segments) in the photoreceptor layer. Segmentation can be challenging when the proximity of cells is small or overlapping. As a result, the density of UV cones reported in the ventral retina is likely an underestimate.

Neighbor density maps and density recovery profiles were generated using the Neighbor density analysis application within the BioVoxxel_Toolbox plugin for ImageJ (imagej.net/plugins/biovoxxel-toolbox). Axis images denoting cell bodies were converted to 8-bit and applied with a binary threshold. Particle neighbor analysis was used to identify the number of cell bodies within a given radius from each soma. Neighbor density maps were generated with density radius of 110µm to approximate the average dendritic diameter of RGCs. Density recovery profiles were calculated similarly using radii from 0 to 400 µm in 20 µm increments. Population per hemisphere were calculated by dividing oriented retinas through the optic nerve head along the naso-temporal axis and

quantifying # of cells per hemisphere. Density of cells per mm^2 was determined by quantifying the number of cells within 1 mm^2 areas of dorsal and ventral retina.

Single cell patch clamp recordings in the retina

Single cell current-clamp recordings were performed in the *GlyT2^{Cre};Ai9* 9 mouse using a HEKA EPC800 amplifier, ITC-18 digitizer and Axograph software. Fluorescent ipRGCs were targeted using brief 554 nm exposure (<100 ms) and a high sensitivity camera (Andor technologies – DU-888E-COO-#BV). Recordings were performed in Ames medium with synaptic blockers 20 µM L-AP4, 25 µM DAP5, 20 µM CNQX to isolate ipRGCs. Five second illumination of blue (445 nm) light was used to elicit intrinsic melanopsin responses at $5x10^{13}$ log photons cm^{-2} s^{-1} using a Texas Instruments DLP4500 LightCrafter projector and custom software (pyStim[90]. Some ipRGCs were targeted for Neurobiotin electroporation using methods described previously[91,92]

Single cell patch clamp recordings monitoring synaptic release in the brain

To study synaptic transmission mediated by the axons of SON-ipRGCs, *GlyT2^{Cre}* mice were crossed with the Ai32 reporter mouse driving channelrodopsin expression in Cre expressing ipRGCs. Male and female *GlyT2^{Cre};Ai32* mice were housed in an environmental chamber (Percival Scientific, Perry, IA) maintained at 20 - 21 ºC on a 12:12 hr light:dark (LD) cycle, with free access to food and water. The ChR2 expressing axonal terminals projecting to the SCN were activated by white light passing through a Chroma excitation filter (BP 470/40). The estimated intensity of the light was 16.5 to 17 log photons cm^{-2} s^{-1}. The ChR2 expressing RHT projection were observed using YFP filter (Chroma, ET-EYFP C212572, Cat.# 49003). The recordings were performed at the end of the day and the beginning of the night. SCN neurons were voltage-clamped in the whole-cell and cell-attached patch clamp modes. The cells were filled with Neurobiotin (0.5%), which made it possible to determine their localization after the experiment. The internal solution consisted of (in mM): 87 CH_3O_3SCs, 15 CsCl, 1 $CaCl_2$, 10 HEPES, 11 EGTA, 31.5 CsOH, 3 MgATP, 0.3 TrisGTP, 10 Phosphocreatine di(tris) salt and 5 N-(2,6-dimethylphenylcarbamoylmethyl)triethylammonium chloride (QX-314); pH 7.25, 278 mOsm. The extracellular recording solution (ACSF) was (in mM): 132.5 NaCl, 2.5 KCl,

1.2 NaH_2PO_4, 2.4 $CaCl_2$, 1.2 $MgCl_2$, 11 glucose, and 22 $NaHCO_3$, saturated with 95% O_2 and 5% CO_2; pH 7.3–7.4, 300–305 mOsm. The equilibrium potential for chloride was -50 mV. For extended detail see Moldavan et al., 2010[93]; 2018[94]. During recordings the inhibitors of glycine, $GABA_A$, and ionotropic glutamate receptors, respectively strychnine (1 μM), gabazine (10 μM), CNQX (20 μM) + AP-5 (DL-AP5, 50 μM), and TTX (1 μM) an inhibitor of voltage-dependent Na^+ currents were applied. EPSCs evoked by electric stimulation of the optic chiasm were also used in order to confirm the recorded cell received retinal inputs.

Contributions

M.H.B, M.M, M.A.M, T.G, O.C, E.W., C.A, HvG and B.S designed and performed experiments and analyzed data, with input from K.W. Confocal microscopy and analysis was performed by M.H.B and B.S., retina patch clamp recordings and dye filling and eye injections were performed by M.H.B, brain injections were performed by O.C., brain slice recordings and optogenetics were performed by M.M, M.A.M, and T.G with help from M.H.B. The manuscript was written by M.H.B and B.S with input from all authors.

Acknowledgments

We would like to thank Alex Tomlinson for help with pyStim, Andre Dagostin help with mouse husbandry and pilot experiments, Lane Brown for help obtaining *OPN4^{Cre}* mice, and Joseph Leffler and David Vaney, and Phyllis Robinson for critically reading the manuscript. This work was supported by EY032564, Lloyd Research Fund, Medical Research Fund of Oregon New Investigator grant P30 EY010572 and unrestricted departmental funding from Research to Prevent Blindness (New York, NY) to BS, NS103842 to CAN, EY031984 to MHB, EY032057 to KW, and acknowledgement is made to the donors of National Glaucoma Research, a program of BrightFocus Foundation, for support of this research.

References

1 Güler, A. D. *et al.* Melanopsin cells are the principal conduits for rod–cone input to non-image-forming vision. *Nature* **453**, 102-105, doi:10.1038/nature06829 (2008).

2 Hatori, M. *et al.* Inducible Ablation of Melanopsin-Expressing Retinal Ganglion Cells Reveals Their Central Role in Non-Image Forming Visual Responses. *PLOS ONE* **3**, e2451, doi:10.1371/journal.pone.0002451 (2008).

3 Hattar, S., Liao, H. W., Takao, M., Berson, D. M. & Yau, K. W. Melanopsin-containing retinal ganglion cells: architecture, projections, and intrinsic photosensitivity. *Science* **295**, 1065-1070, doi:10.1126/science.1069609 (2002).

4 Hattar, S. *et al.* Central projections of melanopsin-expressing retinal ganglion cells in the mouse. *The Journal of comparative neurology* **497**, 326-349, doi:10.1002/cne.20970 (2006).

5 Do, M. T. H. Melanopsin and the Intrinsically Photosensitive Retinal Ganglion Cells: Biophysics to Behavior. *Neuron* **104**, 205-226, doi:10.1016/j.neuron.2019.07.016 (2019).

6 Aranda, M. L. & Schmidt, T. M. Diversity of intrinsically photosensitive retinal ganglion cells: circuits and functions. *Cell Mol Life Sci* **78**, 889-907, doi:10.1007/s00018-020-03641-5 (2021).

7 Berson, D. M., Dunn, F. A. & Takao, M. Phototransduction by retinal ganglion cells that set the circadian clock. *Science* **295**, 1070-1073, doi:10.1126/science.1067262 (2002).

8 Hattar, S. *et al.* Melanopsin and rod-cone photoreceptive systems account for all major accessory visual functions in mice. *Nature* **424**, 76-81, doi:10.1038/nature01761 (2003).

9 Panda, S. *et al.* Melanopsin (Opn4) requirement for normal light-induced circadian phase shifting. *Science* **298**, 2213-2216, doi:10.1126/science.1076848 (2002).

10 Rupp, A. C. *et al.* Distinct ipRGC subpopulations mediate light's acute and circadian effects on body temperature and sleep. *Elife* **8**, doi:10.7554/eLife.44358 (2019).

11 Fernandez, D. C. *et al.* Light Affects Mood and Learning through Distinct Retina-Brain Pathways. *Cell* **175**, 71-84.e18, doi:10.1016/j.cell.2018.08.004 (2018).

12 Sondereker, K. B., Stabio, M. E. & Renna, J. M. Crosstalk: The diversity of melanopsin ganglion cell types has begun to challenge the canonical divide between image-forming and non-image-forming vision. *J Comp Neurol* **528**, 2044-2067, doi:10.1002/cne.24873 (2020).

13 Ebihara, S. & Tsuji, K. Entrainment of the circadian activity rhythm to the light cycle: effective light intensity for a Zeitgeber in the retinal degenerate C3H mouse and the normal C57BL mouse. *Physiol Behav* **24**, 523-527, doi:10.1016/0031-9384(80)90246-2 (1980).

14 Freedman, M. S. *et al.* Regulation of mammalian circadian behavior by non-rod, non-cone, ocular photoreceptors. *Science* **284**, 502-504, doi:10.1126/science.284.5413.502 (1999).

15 Hattar, S. *et al.* Central projections of melanopsin-expressing retinal ganglion cells in the mouse. *J Comp Neurol* **497**, 326-349, doi:10.1002/cne.20970 (2006).

16 Li, J. Y. & Schmidt, T. M. Divergent projection patterns of M1 ipRGC subtypes. *J Comp Neurol* **526**, 2010-2018, doi:10.1002/cne.24469 (2018).

17 Lucas, R. J. *et al.* Diminished pupillary light reflex at high irradiances in melanopsin-knockout mice. *Science* **299**, 245-247, doi:10.1126/science.1077293 (2003).

18 Chen, S. K., Badea, T. C. & Hattar, S. Photoentrainment and pupillary light reflex are mediated by distinct populations of ipRGCs. *Nature* **476**, 92-95, doi:10.1038/nature10206 (2011).

19 Zhao, X., Stafford, B. K., Godin, A. L., King, W. M. & Wong, K. Y. Photoresponse diversity among the five types of intrinsically photosensitive retinal ganglion cells. *The Journal of physiology* **592**, 1619-1636, doi:10.1113/jphysiol.2013.262782 (2014).

20 Keenan, W. T. *et al.* A visual circuit uses complementary mechanisms to support transient and sustained pupil constriction. *Elife* **5**, doi:10.7554/eLife.15392 (2016).

21 Lall, G. S. *et al.* Distinct contributions of rod, cone, and melanopsin photoreceptors to encoding irradiance. *Neuron* **66**, 417-428, doi:10.1016/j.neuron.2010.04.037 (2010).

22 Emanuel, A. J., Kapur, K. & Do, M. T. H. Biophysical Variation within the M1 Type of Ganglion Cell Photoreceptor. *Cell Rep* **21**, 1048-1062, doi:10.1016/j.celrep.2017.09.095 (2017).

23 Milner, E. S. & Do, M. T. H. A Population Representation of Absolute Light Intensity in the Mammalian Retina. *Cell* **171**, 865-876.e816, doi:10.1016/j.cell.2017.09.005 (2017).

24 Dacey, D. M. The mosaic of midget ganglion cells in the human retina. *J Neurosci* **13**, 5334-5355, doi:10.1523/jneurosci.13-12-05334.1993 (1993).

25 Vaney, D. I. Territorial organization of direction-selective ganglion cells in rabbit retina. *J Neurosci* **14**, 6301-6316, doi:10.1523/jneurosci.14-11-06301.1994 (1994).

26 Wassle, H. & Riemann, H. J. The mosaic of nerve cells in the mammalian retina. *Proc R Soc Lond B Biol Sci* **200**, 441-461, doi:10.1098/rspb.1978.0026 (1978).

27 Masland, R. H. The neuronal organization of the retina. *Neuron* **76**, 266-280, doi:10.1016/j.neuron.2012.10.002 (2012).

28 Wassle, H. Parallel processing in the mammalian retina. *Nat Rev Neurosci* **5**, 747-757, doi:10.1038/nrn1497 (2004).

29 Berson, D. M., Castrucci, A. M. & Provencio, I. Morphology and mosaics of melanopsin-expressing retinal ganglion cell types in mice. *The Journal of comparative neurology* **518**, 2405-2422, doi:10.1002/cne.22381 (2010).

30 The Gene Expression Nervous System Atlas (GENSAT) Project, T. R. U. N. Y., NY). MGI download of GENSAT transgene data. *Database Download* (2005).

31 Ishihara, N., Armsen, W., Papadopoulos, T., Betz, H. & Eulenburg, V. Generation of a mouse line expressing Cre recombinase in glycinergic interneurons. *Genesis* **48**, 437-445, doi:10.1002/dvg.20640 (2010).

32 Eulenburg, V. *et al.* GlyT1 determines the glycinergic phenotype of amacrine cells in the mouse retina. *Brain Struct Funct* **223**, 3251-3266, doi:10.1007/s00429-018-1684-3 (2018).

33 Schmidt, T. M., Chen, S. K. & Hattar, S. Intrinsically photosensitive retinal ganglion cells: many subtypes, diverse functions. *Trends Neurosci* **34**, 572-580, doi:10.1016/j.tins.2011.07.001 (2011).

34 Schmidt, T. M. & Kofuji, P. Functional and morphological differences among intrinsically photosensitive retinal ganglion cells. *J Neurosci* **29**, 476-482, doi:10.1523/jneurosci.4117-08.2009 (2009).

35 Schmidt, T. M. & Kofuji, P. Differential cone pathway influence on intrinsically photosensitive retinal ganglion cell subtypes. *J Neurosci* **30**, 16262-16271, doi:10.1523/jneurosci.3656-10.2010 (2010).

36 Schmidt, T. M. & Kofuji, P. Structure and function of bistratified intrinsically photosensitive retinal ganglion cells in the mouse. *Journal of Comparative Neurology* **519**, 1492-1504, doi:10.1002/cne.22579 (2011).

37 Sonoda, T., Okabe, Y. & Schmidt, T. M. Overlapping morphological and functional properties between M4 and M5 intrinsically photosensitive retinal ganglion cells. *The Journal of comparative neurology* **528**, 1028-1040, doi:10.1002/cne.24806 (2020).

38 Estevez, M. E. *et al.* Form and function of the M4 cell, an intrinsically photosensitive retinal ganglion cell type contributing to geniculocortical vision. *J Neurosci* **32**, 13608-13620, doi:10.1523/JNEUROSCI.1422-12.2012 (2012).

39 Baden, T. *et al.* A tale of two retinal domains: near-optimal sampling of achromatic contrasts in natural scenes through asymmetric photoreceptor distribution. *Neuron* **80**, 1206-1217, doi:10.1016/j.neuron.2013.09.030 (2013).

40 Szel, A. *et al.* Unique topographic separation of two spectral classes of cones in the mouse retina. *Journal of Comparative Neurology* **325**, 327-342 (1992).

41 Hannibal, J., Hindersson, P., Knudsen, S. M., Georg, B. & Fahrenkrug, J. The photopigment melanopsin is exclusively present in pituitary adenylate cyclase-activating polypeptide-containing retinal ganglion cells of the retinohypothalamic tract. *J Neurosci* **22**, RC191 (2002).

42 Hughes, S., Watson, Thomas S., Foster, Russell G., Peirson, Stuart N. & Hankins, Mark W. Nonuniform Distribution and Spectral Tuning of Photosensitive Retinal Ganglion Cells of the Mouse Retina. *Current Biology* **23**, 1696-1701, doi:10.1016/j.cub.2013.07.010 (2013).

43 Heukamp, A. S., Warwick, R. A. & Rivlin-Etzion, M. Topographic Variations in Retinal Encoding of Visual Space. *Annu Rev Vis Sci*, doi:10.1146/annurev-vision-121219-081831 (2020).

44 Abrahamson, E. E. & Moore, R. Y. Suprachiasmatic nucleus in the mouse: retinal innervation, intrinsic organization and efferent projections. *Brain Res* **916**, 172-191, doi:10.1016/s0006-8993(01)02890-6 (2001).

45 Moore, R. Y., Speh, J. C. & Leak, R. K. Suprachiasmatic nucleus organization. *Cell Tissue Res* **309**, 89-98, doi:10.1007/s00441-002-0575-2 (2002).

46 Antle, M. C. & Silver, R. Orchestrating time: arrangements of the brain circadian clock. *Trends Neurosci* **28**, 145-151, doi:10.1016/j.tins.2005.01.003 (2005).

47 Yan, L. *et al.* Exploring spatiotemporal organization of SCN circuits. *Cold Spring Harb Symp Quant Biol* **72**, 527-541, doi:10.1101/sqb.2007.72.037 (2007).

48 Varadarajan, S. *et al.* Connectome of the Suprachiasmatic Nucleus: New Evidence of the Core-Shell Relationship. *eNeuro* **5**, doi:10.1523/eneuro.0205-18.2018 (2018).

49 Wen, S. *et al.* Spatiotemporal single-cell analysis of gene expression in the mouse suprachiasmatic nucleus. *Nat Neurosci* **23**, 456-467, doi:10.1038/s41593-020-0586-x (2020).

50 Rothhaas, R. & Chung, S. Role of the Preoptic Area in Sleep and Thermoregulation. *Frontiers in Neuroscience* **15**, doi:10.3389/fnins.2021.664781 (2021).

51 Delville, Y., De Vries, G. J. & Ferris, C. F. Neural connections of the anterior hypothalamus and agonistic behavior in golden hamsters. *Brain Behav Evol* **55**, 53-76, doi:10.1159/000006642 (2000).

52 Ricci, L. A., Schwartzer, J. J. & Melloni, R. H., Jr. Alterations in the anterior hypothalamic dopamine system in aggressive adolescent AAS-treated hamsters. *Horm Behav* **55**, 348-355, doi:10.1016/j.yhbeh.2008.10.011 (2009).

53 Melloni, R. H., Jr. & Ricci, L. A. Adolescent exposure to anabolic/androgenic steroids and the neurobiology of offensive aggression: a hypothalamic neural model based on findings in pubertal Syrian hamsters. *Horm Behav* **58**, 177-191, doi:10.1016/j.yhbeh.2009.11.002 (2010).

54 Zimmerman, C. A., Leib, D. E. & Knight, Z. A. Neural circuits underlying thirst and fluid homeostasis. *Nature reviews. Neuroscience* **18**, 459-469, doi:10.1038/nrn.2017.71 (2017).

55 Biran, J., Tahor, M., Wircer, E. & Levkowitz, G. Role of developmental factors in hypothalamic function. *Front Neuroanat* **9**, 47-47, doi:10.3389/fnana.2015.00047 (2015).

56 Song, Z., Levin, B. E., Stevens, W. & Sladek, C. D. Supraoptic oxytocin and vasopressin neurons function as glucose and metabolic sensors. *Am J Physiol Regul Integr Comp Physiol* **306**, R447-456, doi:10.1152/ajpregu.00520.2013 (2014).

57 Sabatier, N., Leng, G. & Menzies, J. Oxytocin, feeding, and satiety. *Front Endocrinol (Lausanne)* **4**, 35-35, doi:10.3389/fendo.2013.00035 (2013).

58 Armstrong, W. E. & Stern, J. E. Electrophysiological and morphological characteristics of neurons in perinuclear zone of supraoptic nucleus. *Journal of neurophysiology* **78**, 2427-2437, doi:10.1152/jn.1997.78.5.2427 (1997).

59 Ecker, J. L. *et al.* Melanopsin-Expressing Retinal Ganglion-Cell Photoreceptors: Cellular Diversity and Role in Pattern Vision. *Neuron* **67**, 49-60, doi:https://doi.org/10.1016/j.neuron.2010.05.023 (2010).

60 Rodieck, R. W. The density recovery profile: A method for the analysis of points in the plane applicable to retinal studies. *Visual neuroscience* **6**, 95-111, doi:10.1017/S095252380001049X (1991).

61 Zhang, Y., Kim, I. J., Sanes, J. R. & Meister, M. The most numerous ganglion cell type of the mouse retina is a selective feature detector. *Proc Natl Acad Sci U S A* **109**, E2391-2398, doi:10.1073/pnas.1211547109 (2012).

62 Baden, T. *et al.* The functional diversity of retinal ganglion cells in the mouse. *Nature* **529**, 345-350, doi:10.1038/nature16468 (2016).

63 Sonoda, T. *et al.* A noncanonical inhibitory circuit dampens behavioral sensitivity to light. *Science* **368**, 527-531, doi:10.1126/science.aay3152 (2020).

64 Monavarfeshani, A., Sabbagh, U. & Fox, M. A. Not a one-trick pony: Diverse connectivity and functions of the rodent lateral geniculate complex. *Vis Neurosci* **34**, E012, doi:10.1017/S0952523817000098 (2017).

65 Reese, B. E. & Keeley, P. W. Design principles and developmental mechanisms underlying retinal mosaics. *Biol Rev Camb Philos Soc* **90**, 854-876, doi:10.1111/brv.12139 (2015).

66 Wässle, H., Peichl, L. & Boycott, B. B. Dendritic territories of cat retinal ganglion cells. *Nature* **292**, 344-345, doi:10.1038/292344a0 (1981).

67 Do, M. T. *et al.* Photon capture and signalling by melanopsin retinal ganglion cells. *Nature* **457**, 281-287, doi:10.1038/nature07682 (2009).

68 Reese, B. Retinal Mosaics: Pattern Formation Driven by Local Interactions between Homotypic Neighbors. *Frontiers in Neural Circuits* **6**, doi:10.3389/fncir.2012.00024 (2012).

69 Devries, S. H. & Baylor, D. A. Mosaic arrangement of ganglion cell receptive fields in rabbit retina. *Journal of neurophysiology* **78**, 2048-2060, doi:10.1152/jn.1997.78.4.2048 (1997).

70 Fernandez, D. C., Chang, Y.-T., Hattar, S. & Chen, S.-K. Architecture of retinal projections to the central circadian pacemaker. *Proceedings of the National Academy of Sciences* **113**, 6047-6052, doi:10.1073/pnas.1523629113 (2016).

71 Bleckert, A., Schwartz, G. W., Turner, M. H., Rieke, F. & Wong, R. O. Visual space is represented by nonmatching topographies of distinct mouse retinal ganglion cell types. *Curr Biol* **24**, 310-315, doi:10.1016/j.cub.2013.12.020 (2014).

72 Wolfe, J. L. & Tan Summerlin, C. The influence of lunar light on nocturnal activity of the old-field mouse. *Animal Behaviour* **37**, 410-414, doi:https://doi.org/10.1016/0003-3472(89)90088-2 (1989).

73 Upham, N. S. & Hafner, J. C. Do nocturnal rodents in the Great Basin Desert avoid moonlight? *Journal of Mammalogy* **94**, 59-72, doi:10.1644/12-mamm-a-076.1 (2013).

74 Caval-Holme, F., Zhang, Y. & Feller, M. B. Gap Junction Coupling Shapes the Encoding of Light in the Developing Retina. *Current biology : CB* **29**, 4024-4035 e4025, doi:10.1016/j.cub.2019.10.025 (2019).

75 Wilkin, L. D., Mitchell, L. D., Ganten, D. & Johnson, A. K. The supraoptic nucleus: afferents from areas involved in control of body fluid homeostasis. *Neuroscience* **28**, 573-584, doi:10.1016/0306-4522(89)90006-7 (1989).

76 Brown, C. H. Magnocellular Neurons and Posterior Pituitary Function. *Compr Physiol* **6**, 1701-1741, doi:10.1002/cphy.c150053 (2016).

77 Noh, J. Y. *et al.* Circadian rhythms in urinary functions: possible roles of circadian clocks? *Int Neurourol J* **15**, 64-73, doi:10.5213/inj.2011.15.2.64 (2011).

78 Douma, L. G. & Gumz, M. L. Circadian clock-mediated regulation of blood pressure. *Free Radic Biol Med* **119**, 108-114, doi:10.1016/j.freeradbiomed.2017.11.024 (2018).

79 Bertram, R., Helena, C. V., Gonzalez-Iglesias, A. E., Tabak, J. & Freeman, M. E. A tale of two rhythms: the emerging roles of oxytocin in rhythmic prolactin release. *J Neuroendocrinol* **22**, 778-784, doi:10.1111/j.1365-2826.2010.02012.x (2010).

80 Roizen, J., Luedke, C. E., Herzog, E. D. & Muglia, L. J. Oxytocin in the circadian timing of birth. *PloS one* **2**, e922-e922, doi:10.1371/journal.pone.0000922 (2007).

81 van den Pol, A. N. Neuropeptide transmission in brain circuits. *Neuron* **76**, 98-115, doi:10.1016/j.neuron.2012.09.014 (2012).

82 Hannibal, J. *et al.* Gene expression of pituitary adenylate cyclase activating polypeptide (PACAP) in the rat hypothalamus. *Regul Pept* **55**, 133-148, doi:10.1016/0167-0115(94)00099-j (1995).

83 Cagampang, F. R., Piggins, H. D., Sheward, W. J., Harmar, A. J. & Coen, C. W. Circadian changes in PACAP type 1 (PAC1) receptor mRNA in the rat suprachiasmatic and supraoptic nuclei. *Brain Res* **813**, 218-222, doi:10.1016/s0006-8993(98)01044-0 (1998).

84 Herzog, E. D. Neurons and networks in daily rhythms. *Nat Rev Neurosci* **8**, 790-802, doi:10.1038/nrn2215 (2007).

85 Moore, R. Y. in *Progress in Brain Research* Vol. 111 (eds R. M. Buijs *et al.*) 103-119 (Elsevier, 1996).

86 Moga, M. M. & Moore, R. Y. Organization of neural inputs to the suprachiasmatic nucleus in the rat. *Journal of Comparative Neurology* **389**, 508-534 (1997).

87 Moldavan, M., Cravetchi, O. & Allen, C. N. Diurnal properties of tonic and synaptic GABAA receptor-mediated currents in suprachiasmatic nucleus neurons. *J Neurophysiol* **126**, 637-652, doi:10.1152/jn.00556.2020 (2021).

88 Laboulaye, M. A., Duan, X., Qiao, M., Whitney, I. E. & Sanes, J. R. Mapping Transgene Insertion Sites Reveals Complex Interactions Between Mouse Transgenes and Neighboring Endogenous Genes. *Front Mol Neurosci* **11**, 385, doi:10.3389/fnmol.2018.00385 (2018).

89 Arganda-Carreras, I. *et al.* Trainable Weka Segmentation: a machine learning tool for microscopy pixel classification. *Bioinformatics* **33**, 2424-2426, doi:10.1093/bioinformatics/btx180 (2017).

90 Sivyer, B., Tomlinson, A. & Taylor, W. R. Simulated Saccadic Stimuli Suppress ON-Type Direction-Selective Retinal Ganglion Cells via Glycinergic Inhibition. *The Journal of Neuroscience* **39**, 4312-4322, doi:10.1523/jneurosci.3066-18.2019 (2019).

91 Kanjhan, R. & Vaney, D. I. Semi-loose seal Neurobiotin electroporation for combined structural and functional analysis of neurons. *Pflugers Archiv : European journal of physiology* **457**, 561-568, doi:10.1007/s00424-008-0539-9 (2008).

92 Gobran, J. *et al.* Effects of 3D Stratification of Retinal Ganglion Cells in Sholl Analysis. *J Neurosci Methods* **346**, 108907, doi:10.1016/j.jneumeth.2020.108907 (2020).

93 Moldavan, M. G. & Allen, C. N. Retinohypothalamic tract synapses in the rat suprachiasmatic nucleus demonstrate short-term synaptic plasticity. *Journal of neurophysiology* **103**, 2390-2399, doi:10.1152/jn.00695.2009 (2010).

94 Moldavan, M. G., Sollars, P. J., Lasarev, M. R., Allen, C. N. & Pickard, G. E. Circadian Behavioral Responses to Light and Optic Chiasm-Evoked Glutamatergic EPSCs in the Suprachiasmatic Nucleus of ipRGC Conditional vGlut2 Knock-Out Mice. *eNeuro* **5**, ENEURO.0411-0417.2018, doi:10.1523/ENEURO.0411-17.2018 (2018).

A subtype of melanopsin ganglion cells encodes ground luminance

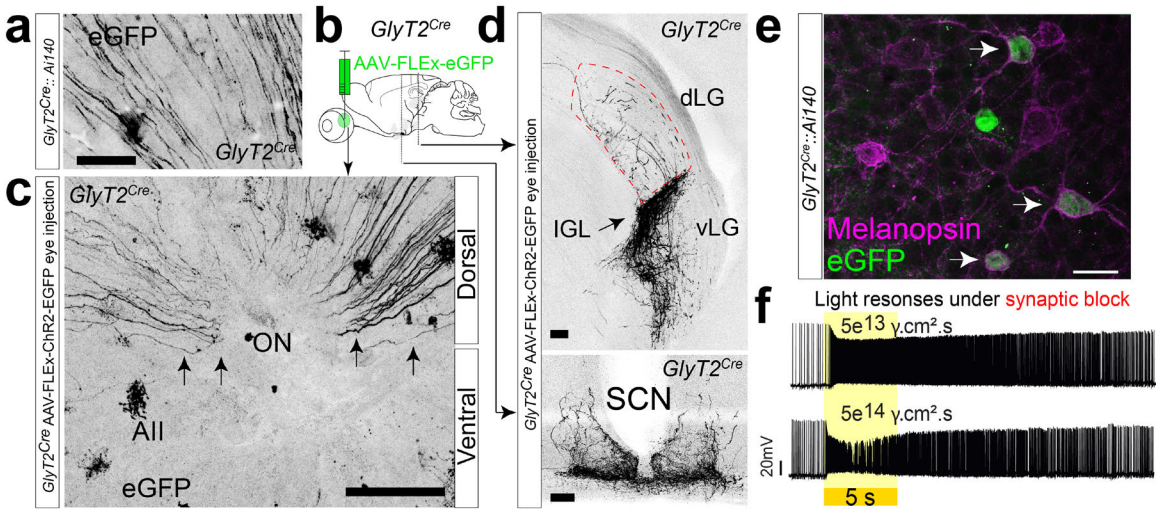

Figure 1: A subpopulation of ipRGCs in dorsal retina
(a) RGC axons identified in the dorsal portion of *GlyT2^{Cre};Ai140* whole mount retina. **(b-d)** Cre-dependent virus injection into the eyes of *GlyT2^{Cre}* mice label RGC axons that project from the dorsal retina via the optic nerve (ON) **(c)** to non-image forming central areas **(d)**: Intergeniculate leaflet (IGL; top) and suprachiasmatic nucleus (SCN; bottom; dLG & vLG = dorsal & ventral lateral geniculate nucleus**. (e)** Confocal micrographs of melanopsin antibody staining (magenta) in *GlyT2^{Cre}*;Ai140 mice labelling cells with eGFP (green). **(f)** Current clamp recordings of light responses to 5 sec visual stimuli under synaptic block (20 µM L-AP4, 25 µM DAP5, 20 µM CNQX) illustrate *GlyT2^{Cre}*-positive RGCs are intrinsically photosensitive (ipRGCs). Scale bar in a = 20 µm, c = 100 µm, d = 100 µm, e = 20 µm.

A subtype of melanopsin ganglion cells encodes ground luminance

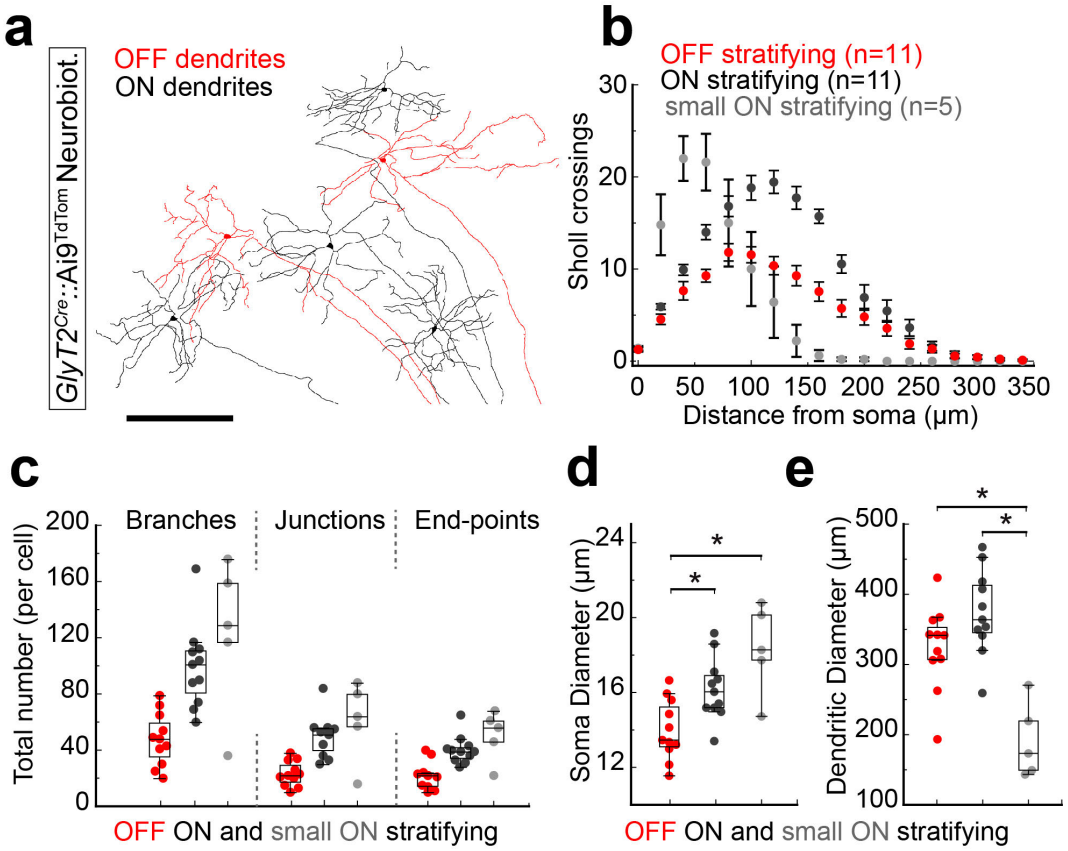

Figure 2: Dendritic morphology of *GlyT2*^{Cre} ipRGCs

(a) Tracings of Neurobiotin electroporated *GlyT2*^{Cre} ipRGCs illustrate multiple morphological subtypes with dendritic stratification in the OFF (red) or ON (black) layers of the inner plexiform layer (IPL). **(b)** Dendritic crossings at radial distances from each soma (Sholl analysis) **(c)**, number of branches, junctions and end-points, as well as total soma **(d)** and dendritic diameter **(e)** quantified per morphologically distinct subpopulation. n = 11 OFF stratifying ipRGCs (M1), 11 ON or partially bi-stratified, and 5 small ON stratifying cells (mixed ON stratifying/non-M1 ipRGCs). Values are mean±SEM. Statistical significance assessed using one-way Anova with Bonferroni correction for comparisons between multiple groups (*$p \leq 0.05$). Scale bar = (a);300 µm

A subtype of melanopsin ganglion cells encodes ground luminance

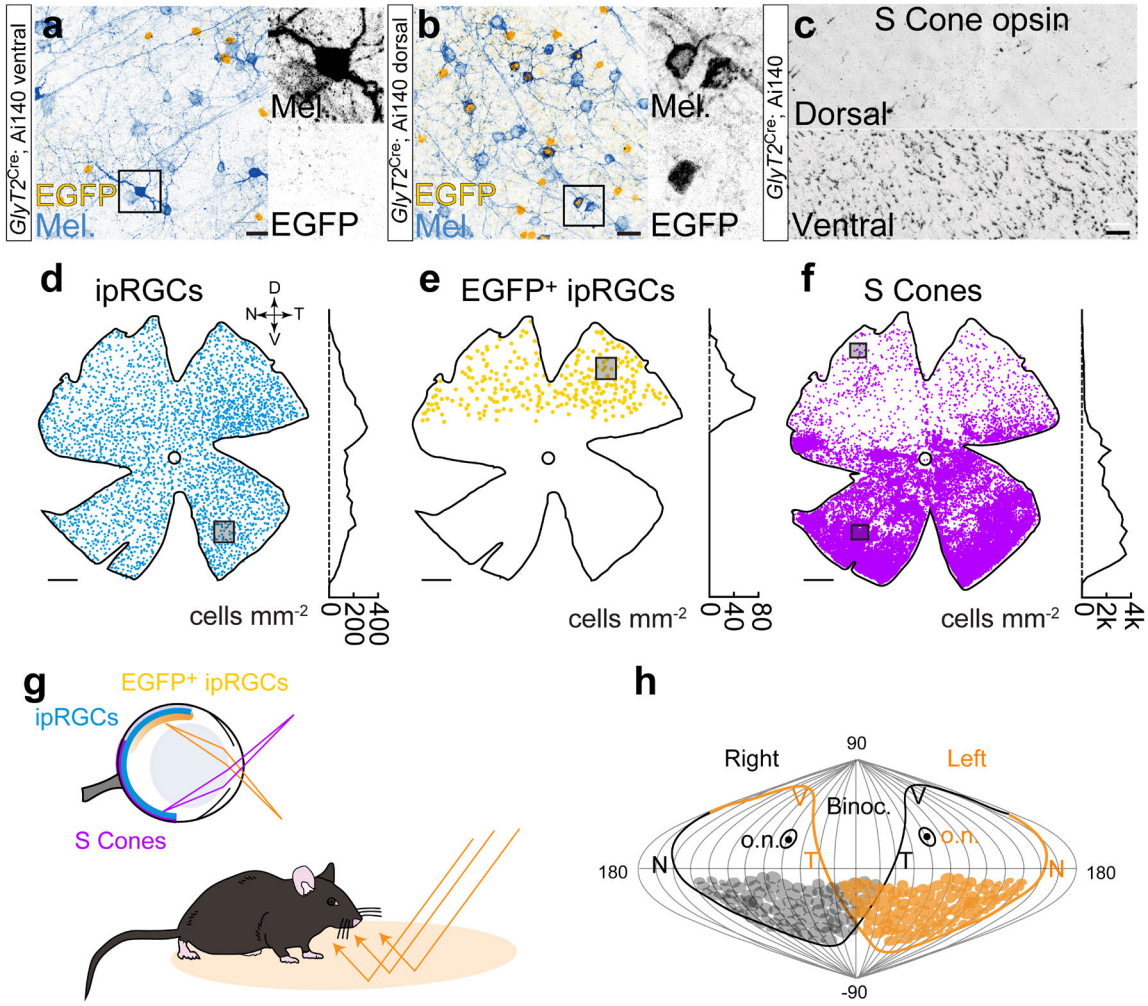

Figure 3: Localized distribution of *GlyT2Cre* positive ipRGCs capture reflected light Confocal micrographs and density maps of neurons labeled in *GlyT2*^{Cre} mice. **(a)** Melanopsin positive ipRGCs in the ventral retina are negative for EGFP. **(b)** In the dorsal retina many ipRGCs are EGFP positive and overlap with EGFP-negative ipRGCs. **(c)** Antibody staining for mouse S-cone opsin illustrates sparse labelling in the dorsal retina and dense staining in the ventral retina. **(d)** Location map of n = 3314 melanopsin immuno-positive ipRGCs throughout the retina. Density at each retinal location along the dorso-ventral axis is plotted on the right (100 µm bins across the Y axis) illustrating the higher density of ipRGCs in the dorsal retina. Square = region in a. **(e)** 293 ipRGCs were EGFP-positive and restricted to a region of retina that is low in **(f)** S cone opsin density. Squares = regions in b, and c above, respectively. **(g)** Illustration of the *GlyT2*^{Cre} ipRGCs in the dorsal retina of the mouse encoding light in the ventral visual field (reflected off the ground), High density of S cones aligned with the dorsal visual field (purple). Purple = density of S cones, blue = all ipRGCs, orange = *GlyT2Cre* ipRGCs. **(h)** Distribution of *GlyT2*^{Cre} ipRGCs in both eyes plotted in a sinusoidal projection adapted from Bleckert et al. 2014[1]. Orange outline = edge of left retina; black outline = edge of right retina. on = optic nerve. D = dorsal, V = ventral, N = nasal, T = temporal. Scale bars in (a,b,c) 25 µm, (d,e,f); 0.5 mm.

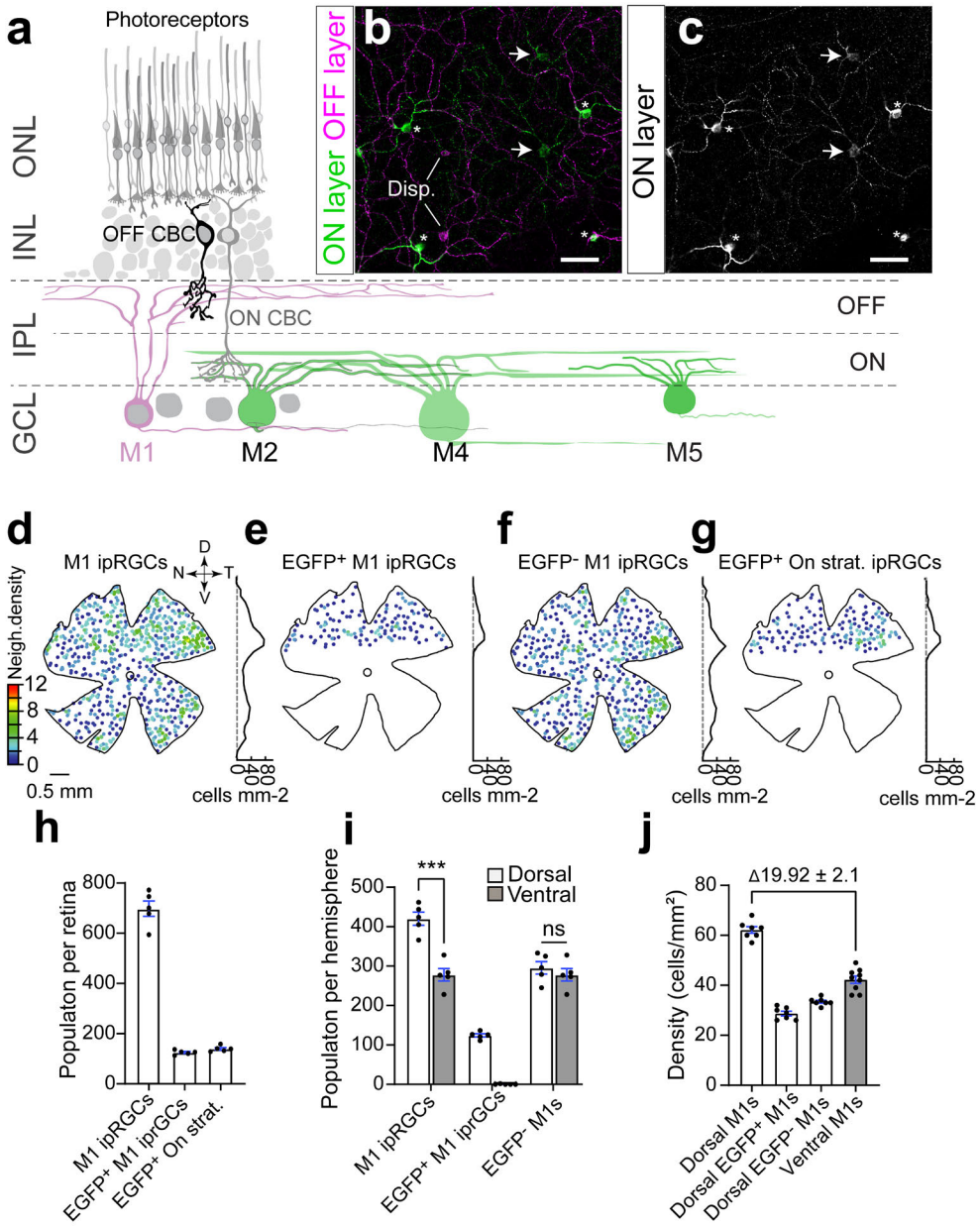

Figure 4: An additional M1 ipRGC visual channel dedicated to the dorsal retina
(**a**) Schematic of the retinal circuit with rod and cone photoreceptors located in the outer nuclear layer (ONL) and photosensitive ipRGCs in the ganglion cell layer (GCL). Some of the 6 ipRGC types (bistratified ipRGCs excluded) differ in their dendritic size and stratification in the ON (green) and OFF (magenta) inner plexiform layer (IPL). (**b-c**) confocal micrographs of ipRGCs stain with melanopsin antibody illustrating M1 ipRGCs (asterisks) identified as their dendrites clearly transition to from the ON layer (b; green; c) to the OFF layer (b; magenta). ON ipRGCs can be identified by their primary dendrites branching in the ON layer (arrows in b,c) **(d)** Neighbor density maps of morphologically identified M1 ipRGCs (melanopsin+), **(e)** EGFP$^+$ M1 ipRGCs, (**f**) EGFP$^-$ M1 ipRGCs, and **(g)** EGFP$^+$ On stratifying ipRGCs. Each cell is color coded according to the number of neighboring cells within a diameter of 220 µm. Hotter colored cells lie within regions of higher density such as the dorsal retina for all M1 ipRGCs and the temporal retina for

EGFP- M1 ipRGCs **(h)** Bar graph of quantified M1 ipRGCs, $EGFP^+$ M1 ipRGCs, and ON stratifying $EGFP^+$ ipRGCs in retina whole mount. (**i**) Population per hemisphere and (**j**) density (dorsal; white vs. ventral; gray) for morphologically identified M1 ipRGCs per 1 mm^{-2}. $EGFP^-$M1s = (All) M1 ipRGCs - $EGFP^+$M1 ipRGCs. Values are mean ± SEM. Statistical significance assessed using one-way Anova. *** = $p < 0.001$, n = 4 retina. Scale bar in (b) and (c) = 50 µm.

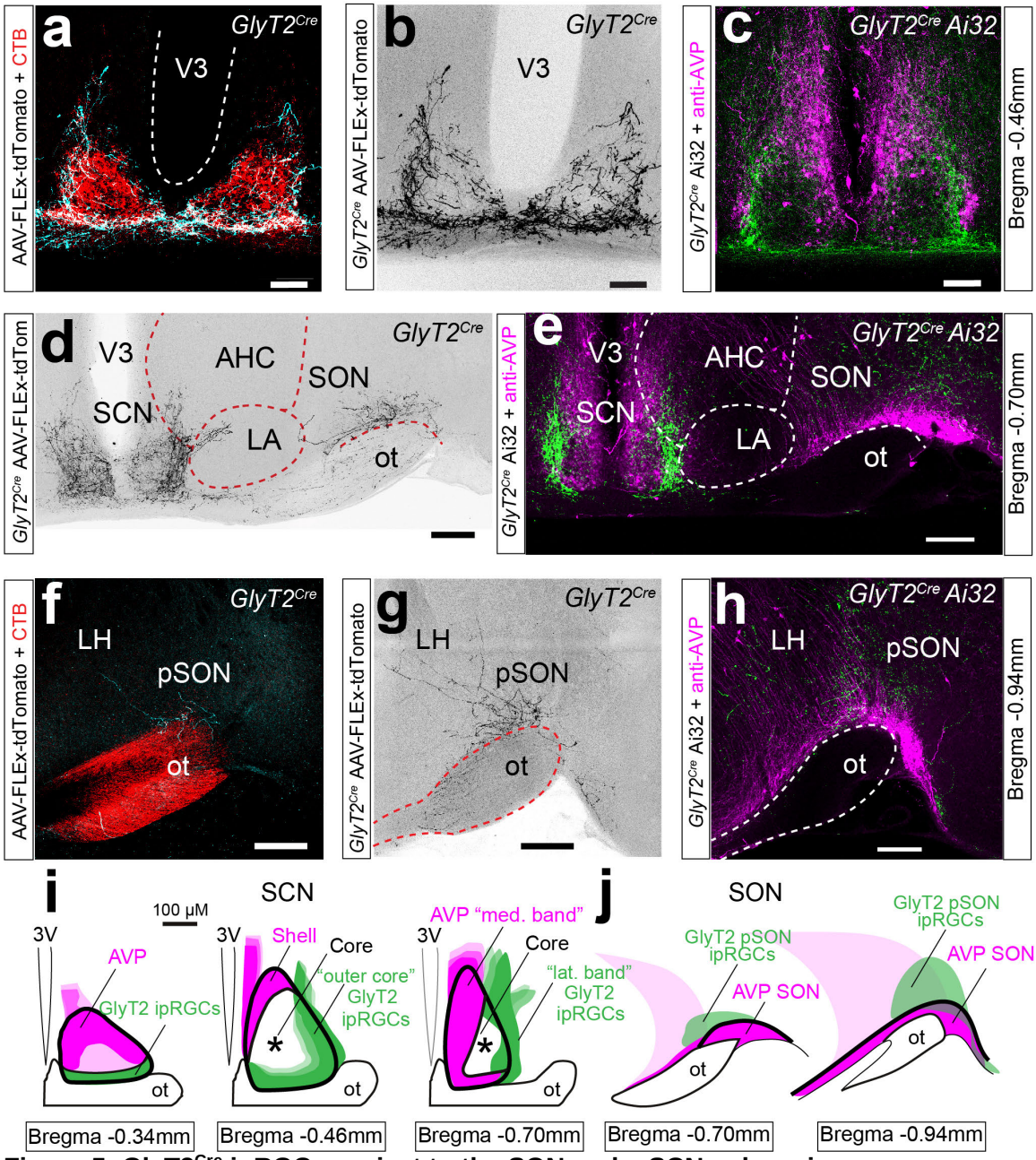

Figure 5: GlyT2^{Cre} ipRGCs project to the SON and a SCN sub-region

(a-n) Intravitreal eye injections of Cre-dependent AAV (AAV-FLEX-tdTomato) in the *GlyT2^{Cre}* mouse allowed anterograde tracing of central projections in confocal images of coronal 200 µm brain sections. Cholera toxin subunit B (CTB), was co-injected to label all RGC axons. **(a-b)** The SCN receives dense ipRGC input at its central core (a – red) *GlyT2^{Cre}* ipRGCs (blue) largely avoid the central core and instead innervate the outer core in the rostral SCN and form a lateral band in the caudal SCN. **(c)** Outer core and lateral band localized in the *GlyT2^{Cre};Ai32* (green = YFP of *GlyT2^{Cre}* ipRGC terminals) is distinct from the anatomical shell of the SCN localized by arginine vasopressin neurons (AVP – magenta). (**d,e**) In the caudal SCN the lateral band extends into lateral hypothalamic (LA)

and anterior hypothalamic (AHC) areas in eye injected *GlyT2^{Cre}* (d) and GlyT2^{Cre}:Ai32 mice (e). **(d-h)** GlyT2^{Cre} ipRGCs innervate the supraoptic nucleus (SON) observed in eye injected GlyT2^{Cre} (d,f,g) and *GlyT2^{Cre};Ai32* mice (e,h) superior to the dense AVP-positive cell bodies of the SON (magenta). **(i,j)** Summary illustrations of *GlyT2^{Cre}* ipRGC projections (green) to the (i) SCN outer core and SCN lateral band as well as projections to the (j) SON, superior to the dense AVP+ cell bodies (magenta). Anatomical distances from bregma determined from the Franklin & Paxinos Mouse Brain Coordinate Atlas. Scale bar = (a-c,i);100 µm, (d-h); 200 µm.

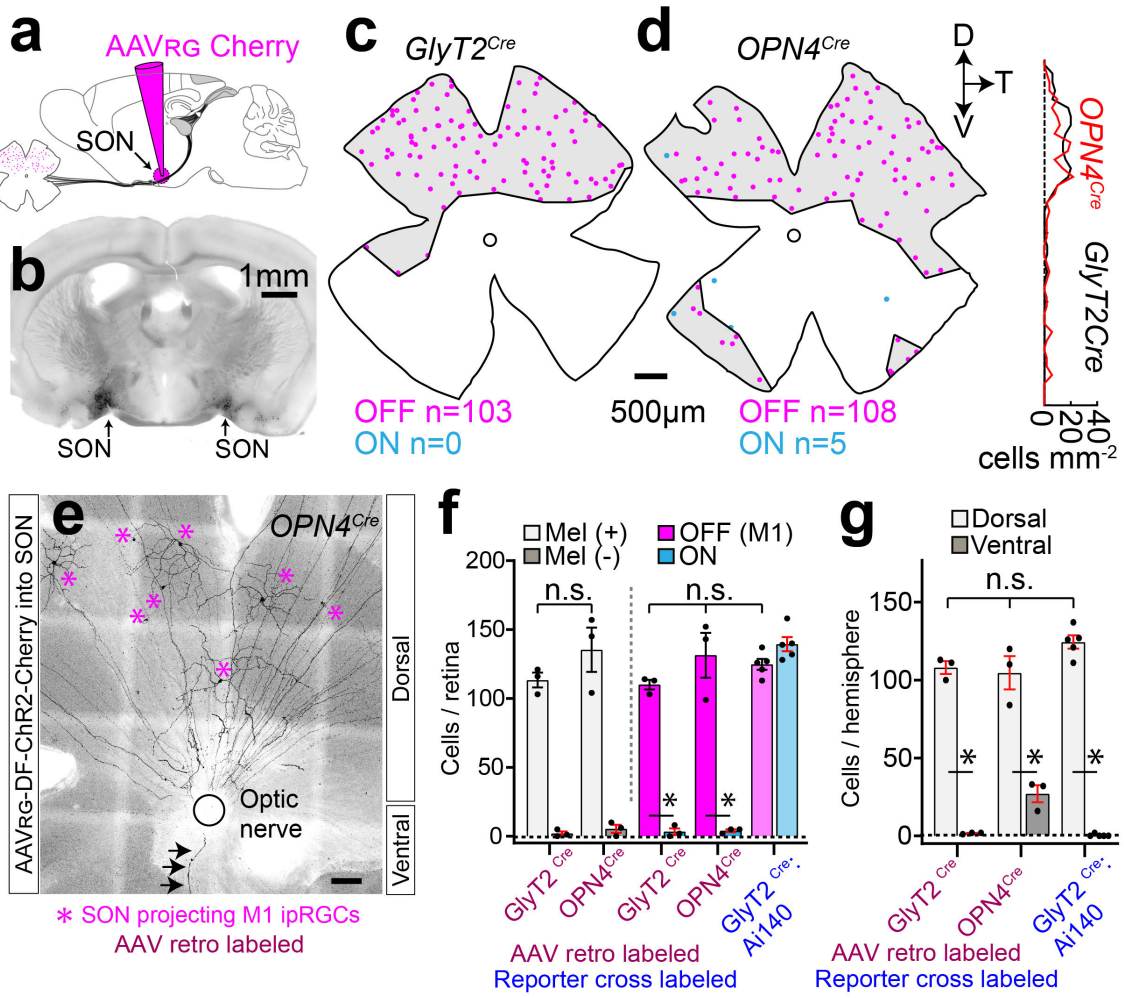

Figure 6: *GlyT2*^{Cre} ipRGCs form the principle projection to the SON

(a,b) Stereotactic injections of Cre-dependent retroAAV (magenta) into the SON (b) labels (**c,d**) a population of M1 ipRGCs (OFF stratifying; magenta) in the *GlyT2*^{Cre} **(c)** and *OPN4*^{cre} **(d)** mouse lines. Density at each retinal location along the dorso-ventral axis is plotted on the right. **(e)** Confocal image of the flat mount retina illustrates that retro-labeled M1 ipRGCs in the *OPN4*^{Cre} localize to the dorsal retina, black arrows indicate a rare ventral axon. **(f)** Bar graphs of ipRGCs per retina that are melanopsin positive (white) or negative (gray) (left) and either OFF (M1, magenta) or ON (turquoise) stratifying ipRGCs (right) in SON injected *GlyT2*^{Cre} and *OPN4*^{Cre} mice retinas (AAV retro labeled; maroon). *GlyT2*^{Cre}*;Ai140* retinas quantified for comparison (l - far right, Reporter cross labeled; blue). **(g)** Bar graphs of population of cells per hemisphere in the SON injected *GlyT2*^{Cre} and *OPN4*^{Cre} mouse retinas. *GlyT2*^{Cre}*;Ai140* retinas quantified for comparison (g - far right). Values are mean±SEM. Statistical significance assessed using one-way Anova with Bonferroni correction for comparisons between multiple groups (*$p \leq 0.01$) Scale bar = (a); 1mm, (c,d); 500 µm,(e);100 µm.

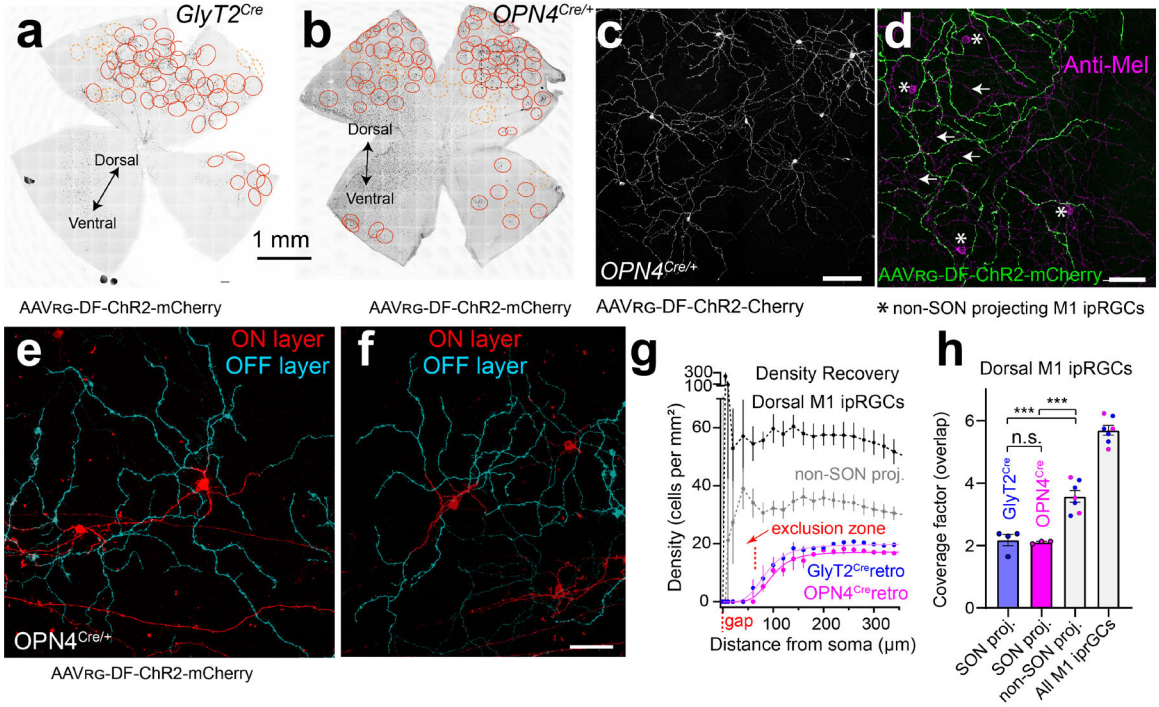

Figure 7: SON ipRGCs form a tiling mosaic that minimizes dendritic overlap. Whole retina images of tiling SON M1 ipRGCs retro-labeled in the *GlyT2^{Cre}* **(a)** and *OPN4^{Cre}* **(b)** with dendritic arbor circled in red. (c) Confocal images of mosaic spacing in SON M1 ipRGCs labeled in the *OPN4^{Cre}*. **(d)** Higher magnification confocal image of OFF stratifying dendrites (green) which overlap with surrounding M1 ipRGCs dendrites stained with anti-melanopsin (magenta; arrows). Some displaced M1 ipRGC cell bodies (asterisk) are not labeled in the SON injection. **(e,f)** Dendritic morphology of SON M1 ipRGCs illustrate they have 3-4 short dendritic segments in the ON layer (red) that dive into their terminal dendrites in the OFF layer (cyan). **(g)** Density recovery profile displaying density of cell bodies at distances (µm) from each soma. Gap (red) indicates minimal overlap of SON ipRGCs in the SON-injected *GlyT2^{Cre}* and *OPN4^{Cre}* retina. **(h)** Coverage factor or the proportion of dendritic overlap calculated from the average diameter of M1 ipRGCs, measured from Neurobiotin fills. Non-SON proj. M1s (grey) = M1 ipRGCs not labeled in the central injection. Dorsal M1s = Non-SON projecting M1s + retro labeled (SON projecting) M1s. Statistical significance assessed using one-way Anova with Bonferroni correction for comparisons between multiple groups (***$p \leq 0.001$) Scale bar = (a,b); 1mm, (c); 100 µm,(d-f); 50 µm.

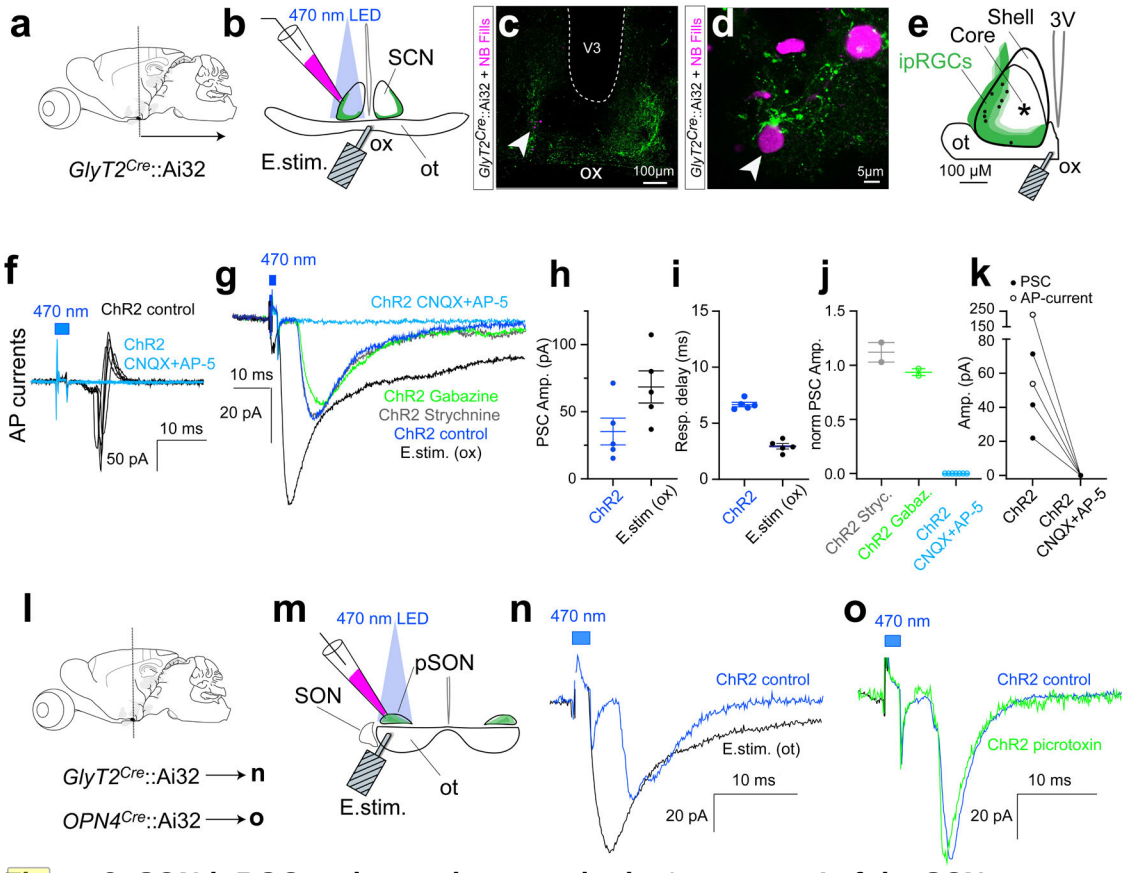

Figure 8: SON-ipRGCs release glutamate in the 'outer core' of the SCN

(a,b) Brain slice recordings in the SCN were performed in coronal sections of *GlyT2^{Cre};Ai32* mice. Patch electrode prefilled with Neurobiotin (magenta) and electrical stimulating electrode placed in the optic chiasm (ox; E.stim) in order to stimulate retinal axons. **(c)** Confocal images of SCN slice, immunostained following recordings. **(d)** Recorded cells localized with Neurobiotin in close proximity to SON-ipRGC terminals. **(e)** Location of the photo-responsive cells (black dots) relative to SON-ipRGC central innervation of the SCN outer core (green). **(f)** Photo-stimulation evoked action potential currents (black) are abolished following bath application of CNQX + AP-5 (light blue). **(g)** Whole cell voltage clamp recording traces of electrical (black) and channelrhodopsin-evoked (ChR2) inward post-synaptic currents (PSCs) in control (dark blue), 1 µM strychnine (grey), 10 µM SR-95531 (green). ChR2-evoked currents were abolished with CNQX (20 µM) and AP-5 (50 µM; light blue). **(h)** Response amplitude and (**i**) delay of ChR2- evoked (right) and electrical stimulation evoked (E.Stim) PSCs in the same SCN neurons. (**j**) ChR2-evoked response amplitude in strychnine (grey), SR-95531 (green), or CNQX + AP-5 (light blue) normalized to the control response amplitude. Values are mean ± SEM. **(k)** PSC amplitude before and after CNQX + AP-5. **(l, m)** Coronal brain slices were used for recordings in the SON of the *GlyT2^{Cre};Ai32* mouse and *OPN4^{Cre};Ai32* mouse. **(n)** Whole cell voltage clamp recording traces of electrical (black) and ChR2-evoked inward post-synaptic currents (PSCs) (blue) in the SON. **(o)** Voltage clamp recording traces of ChR2-evoked inward post-synaptic currents (PSCs) in the SON before (blue) and after (green) 50 µM picrotoxin. Statistical significance assessed using one-way Anova with Sidak correction for comparisons between multiple groups (*$p \leq 0.01$). Scale bar = (c); 100 µm, (d); 5 µm.

A subtype of melanopsin ganglion cells encodes ground luminance

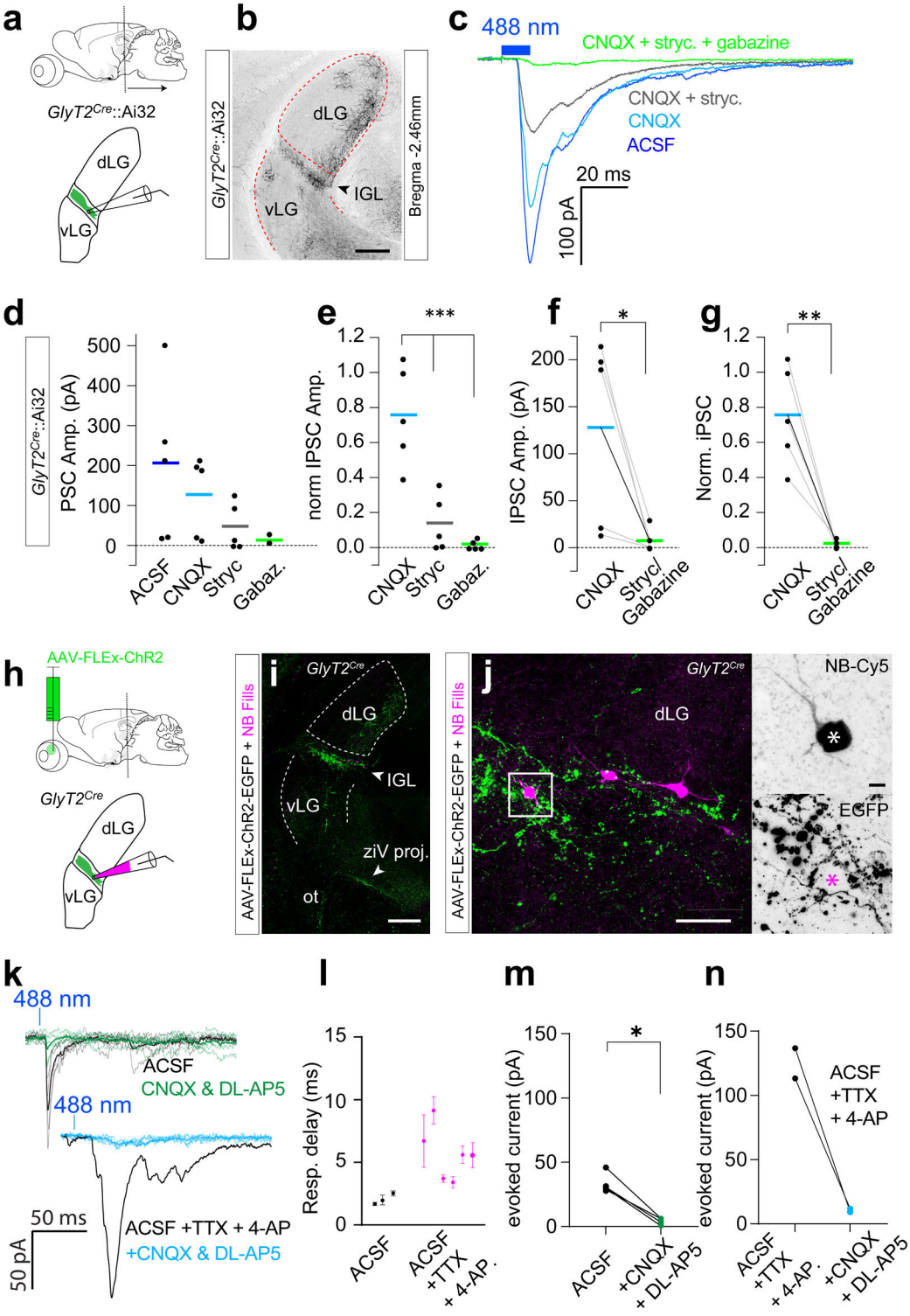

Figure 9: SON-ipRGCs release glutamate at the IGL

(a) Coronal sections were used for brain slice recordings in the IGL of the *GlyT2^{Cre};Ai32* mouse. **(b)** Confocal image of the ventral lateral geniculate nucleus (vLG), intergeniculate

leaflet (IGL), and the dorsal lateral geniculate nucleus (dLG) illustrating EYFP expression in *GlyT2^{Cre};Ai32* brain. **(c)** Whole cell voltage clamp recording traces of photo-stimulation under Control (blue), 20 µM CNQX (light blue), 0.5 µM strychnine + CNQX (gray), and 3 µM gabazine + strychnine + CNQX (green). **(d,e)** Photo-response amplitude (d) and normalized photo-response amplitude (e) of PSC under blocker conditions. **(f,g)** Photo-response amplitude (f) and normalized photo-response amplitude (g) in CNQX before and after the addition of gabazine + strychnine. **(h)** Illustration of brain slice recordings in the IGL of the *GlyT2^{Cre}* mouse 3wks following Cre-dependent ChR2 expression in the eye. **(i-j)** Confocal images of EGFP expression in the IGL brain slice, fixed after recording. Biocytin filled IGL neuron (magenta) surrounded by SON-ipRGC terminals (green). **(k)** (k -top) Photo-stimulation evoked inward PSCs (black) that were blocked by excitatory neurotransmitters CNQX and DL-AP5 (green). (k – bottom) Photo-stimulation evoked inward PSCs (black) in tetrodotoxin and 4-aminopyridine were blocked with co-application of CNQX and DL-AP5 (blue).(l) Response delay indicating the time to peak following a 1 ms ChR2 stimulation in ACSF (black; n = 3 cells mean ± SEM between trials), and following the application of TTX and 4-AP (magenta, n = 5, mean ± SEM between trials) **(m)** Amplitude of photo-induced PSC in ACSF before and after CNQX and DL-AP5. b Amplitude of photo-induced PSC in ACSF with TTX and 4-AP before and after CNQX and DL-AP5. Statistical significance assessed using one-way Anova with Holm-Sidaks correction for multiple comparisons (***$p \leq 0.001$). Scale bar = (a,i); 250 µm, (j); 50 µm.

A subtype of melanopsin ganglion cells encodes ground luminance

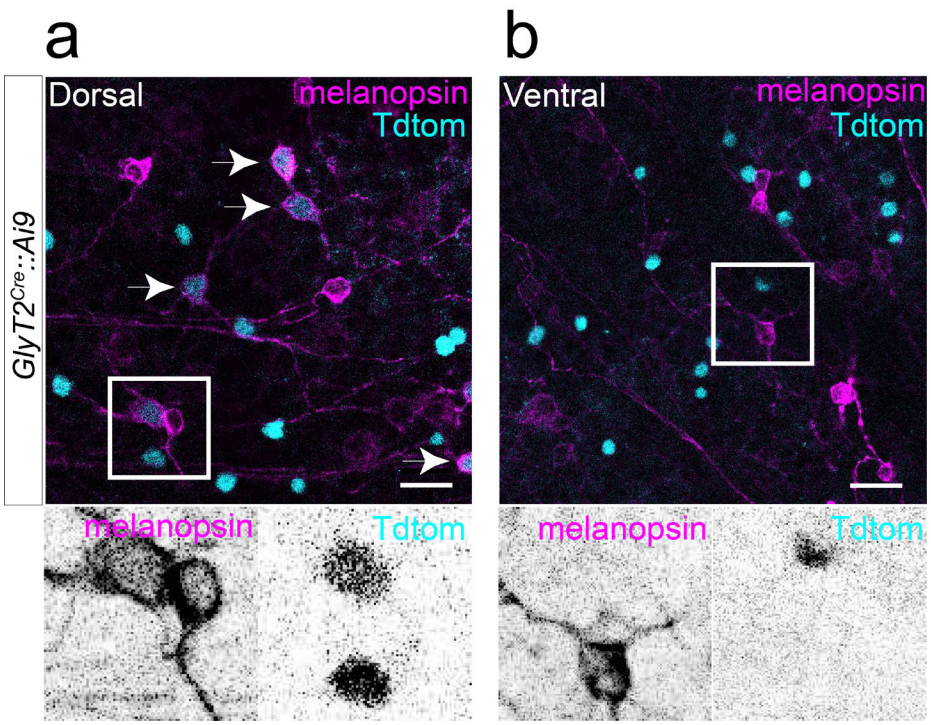

Supplementary Figure 1: Fluorescent IpRGCs in the dorsal retina of the *GlyT2^{Cre};Ai9* mice.
Confocal images of melanopsin expressing (magenta) Tdtomato+ (cyan) ipRGCs in the dorsal **(a)** but not the ventral **(b)** hemisphere of the wholemount retina of the *GlyT2^{Cre};Ai9* mouse. Scale bar = (a,b); 25 µm.

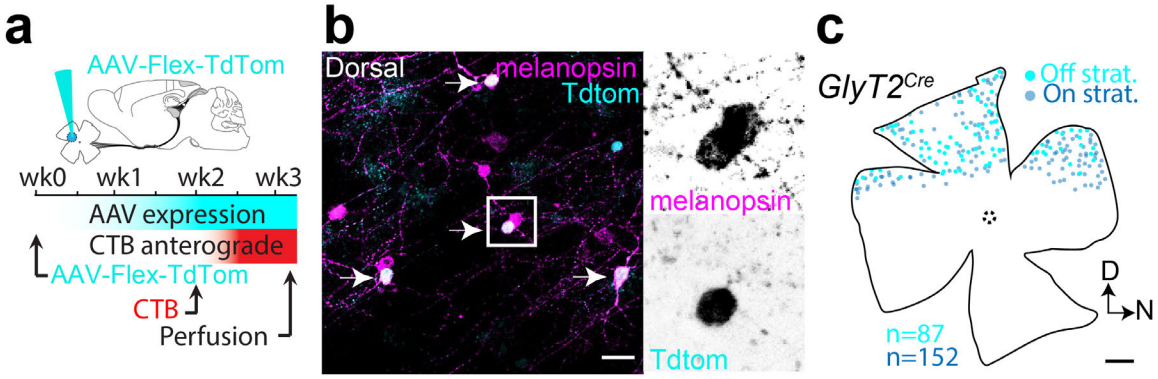

Supplementary Figure 2: Cre-dependent anterograde AAV labeling strategy
(a) Anterograde eye injection protocol used for identifying the central projections of *GlyT2^{Cre}* ipRGCs (Cre-dependent AAV – TdTomato; cyan) among RGC recipient areas (CTB labeling of all RGC axons, red). **(b)** A Cre-dependent AAV was used to drive fluorescent TdTomato expression (cyan) in the *Cre*+ retinal neurons. Melanopsin (magenta) staining confirmed that all virally labeled RGCs are ipRGCs (white). **(c)** Retina map and subtype distribution of AAV labeled GlyT2^{Cre} ipRGCs in the retina. OFF stratified (cyan) and ON stratified (blue) refers to the layer of the inner plexiform layer (INL) in which the dendrites terminate. Scale bars: (b); 25 µm. (c); 500 µm.

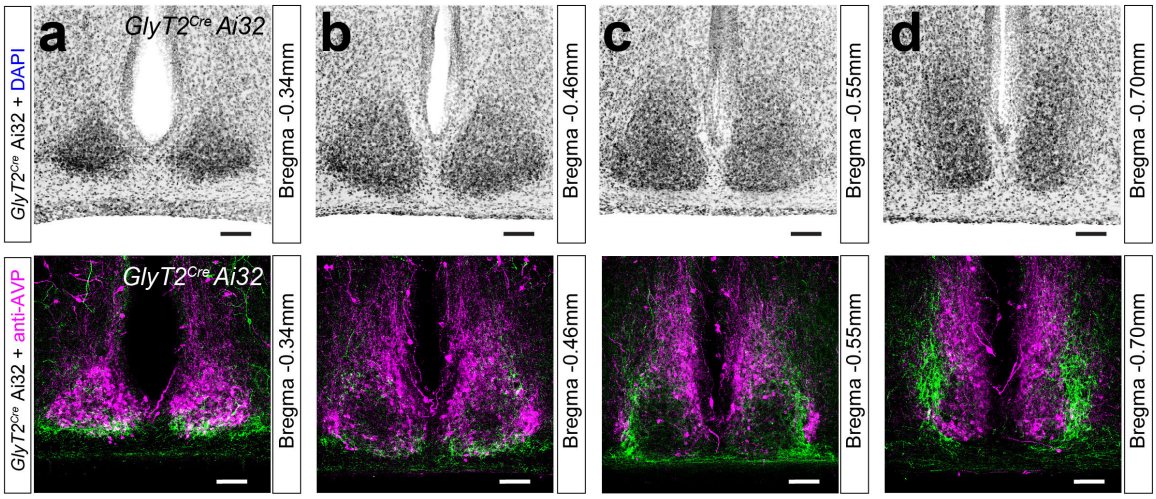

Supplementary Figure 3: Distinct anatomical areas of the SCN innervated by axons from *GlyT2*^{Cre} ipRGCs
Coronal sections of the SCN of a *GlyT2*^{Cre}*;Ai32* mouse, presented anterior to posterior. EYFP-expressing *GlyT2*^{Cre} ipRGCs (bottom - green) innervate previously undescribed locations of the SCN we call the outer core and lateral band, avoiding the SCN shell defined by AVP staining (bottom - magenta). DAPI (top) provides an anatomical reference. Scale bars: (a-d); 100 µm.

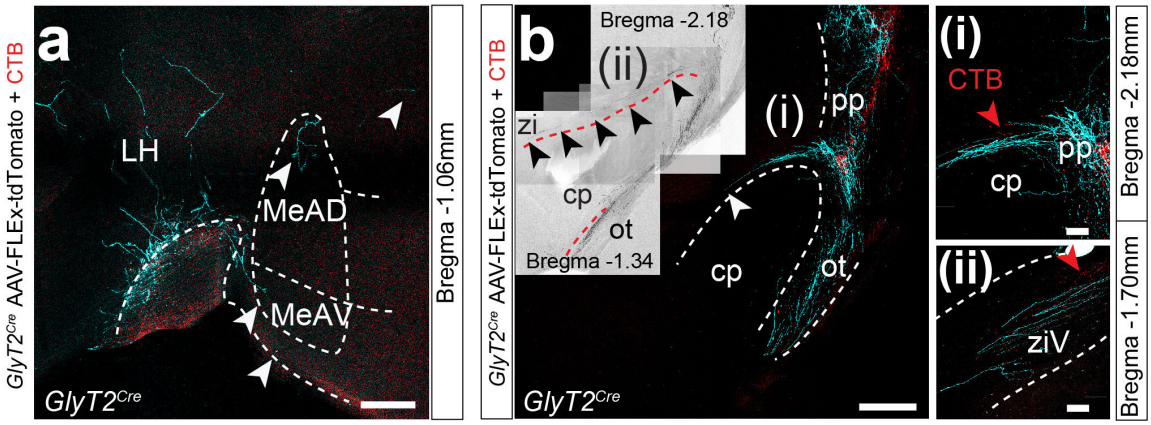

Supplementary Figure 4: Other sites of hypothalamic projection
(a) Cre-dependent AAV (AAV-FLEX-tdTomato) eye injection in the *GlyT2*^{Cre} mouse also labeled sparse projections in the lateral hypothalamus and in the anteroventral and anterodorsal edges of the medial amygdalar nucleus (MeAD & MeAV). **(b)** At the level the rostral ventral lateral geniculate nucleus (vLGN), before entering the geniculate complex, *GlyT2*^{Cre} ipRGCs emerge from the optic tract and split at the peripeduncular nucleus (pp) (n(i)). A moderate number of ventromedial axons wrap around the cerebral peduncle (cp) and project nearly 1mm caudally along the ventral length of the zona incerta (ziV) (i,ii = inlay from n) (red arrow denotes presence of CTB). The function of the zona incerta is unknown. Scale bars: (a,b); 200 µm, (i,ii); 50 µm.

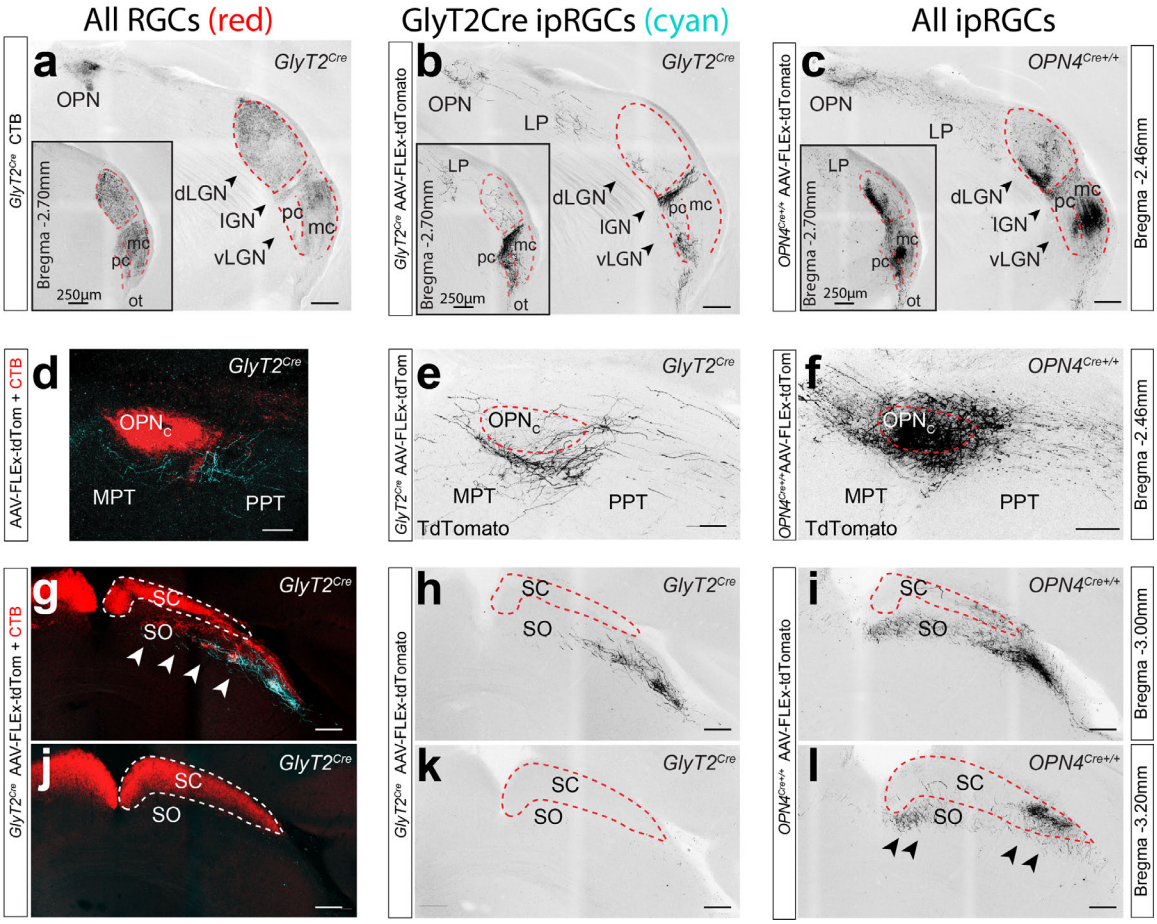

Supplementary Figure 5: Thalamic, pretectal, and collicular ipRGC projections Anterograde tracing of central projections in *GlyT2*^{Cre} and *OPN4*^{Cre} mouse lines following intravitreal eye injections with Cre-dependent AAV (AAV-FLEX-tdTomato). Cholera toxin subunit B (CTB), which labels all RGC axons, was used for anatomical assistance (a,d,j – red). **(a-c)** Confocal images of coronal brain slice reveal that ipRGCs labeled in the *GlyT2*^{Cre} innervate the parvocellular (pc) division of the ventrolateral geniculate complex (vLGN) and the intergeniculate leaflet (IGL) **(b)** IpRGCs labeled in the *OPN4*^{Cre} more broadly innervate the parvocellular (pc) and magnocellular (mc) divisions of the vLGN, IGL, and focal portions of the dorsolateral geniculate complex (dLGN) **(c)** *GlyT2*^{Cre} ipRGCs also form a plexus of terminals in the lateral posterior nucleus (LP). **(d-f)** Confocal images of the olivary pretectal nucleus (OPN) identify that *GlyT2*^{Cre} ipRGCs innervate the ventral cup of the OPN shell, where ipRGCs labeled in the *OPN4*^{Cre} project to both core and shell regions, similar to that observed by CTB labeling (d – red). Sparse innervation to neighboring pretectal structures such as medial pretectal (MPT) and posterior pretectal (PPT) areas are also observed. **(g-l)** Confocal images of the superior colliculus (SC), reveal that *GlyT2*^{Cre} ipRGCs have some innervation to the superior colliculus (SC) **(h)**, like many ipRGCs and RGCs (g,i,j,l). These projections are sparse and localized to the superficial layer of the stratum opticum (SO) (h), with very few projections to the central SC, unlike those in the OPN4Cre or the CTB labeling (d –red). Scale bars: (a-c,g-l); 250 µm, (d-f); 100 µm.

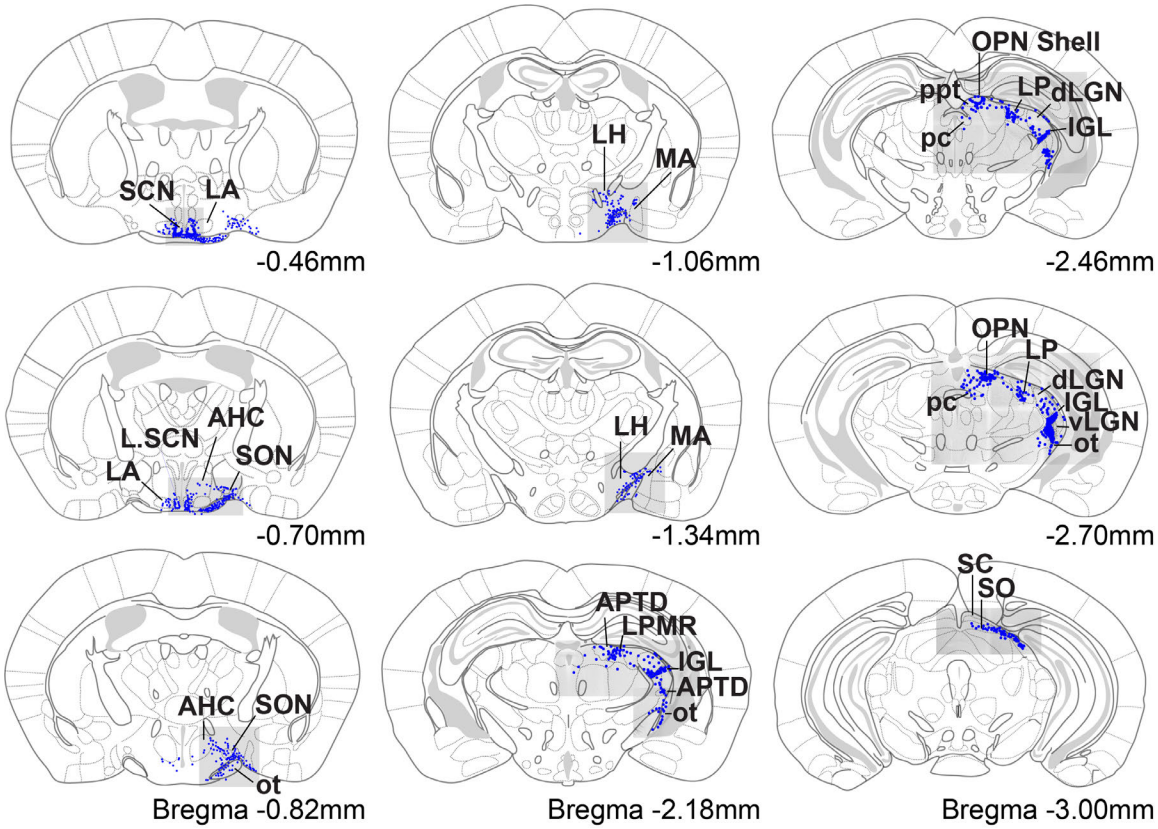

Supplementary Figure 6: Summary of ipRGC central projections in the *GlyT2*^{Cre} mouse

Graphical atlas maps (blue: axons and terminals) drawn from the brain slices of *GlyT2*^{Cre} mice using the Franklin & Paxinos Mouse Brain Coordinate Atlas. suprachiasmatic nucleus (SCN) supraoptic nucleus (SON), optic tract (ot), lateral anterior hypothalamic (LA), anterior hypothalamic (AHC), lateral hypothalamus (LH), Medial amygdalar nucleus (MA) superior colliculus (SC), stratum opticum (SO), posterior pretectal area (PPT), olivery pretectal nucleus core & shell (OPN), ventrolateral geniculate complex (vLGN), intergeniculate leaflet (IGL), lateral posterior nucleus (LP), dorsolateral geniculate complex (dLGN).

A subtype of melanopsin ganglion cells encodes ground luminance

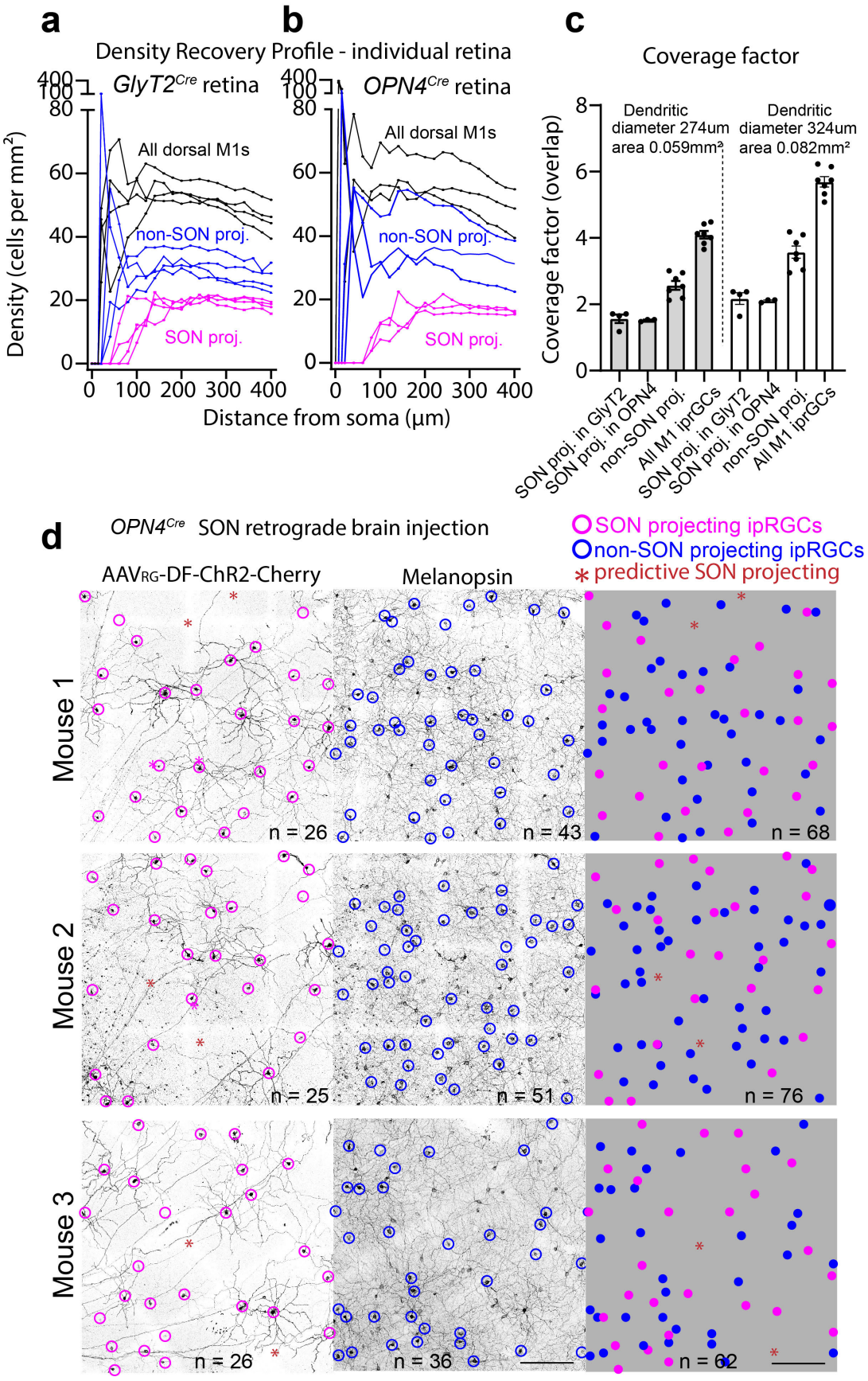

Supplementary Figure 7: Stereotactic SON injection identifies M1 GlyT2 ipRGCs

(a,b) Density recovery profile (per retina) of dorsal M1 ipRGCs labeled by central injection (SON) in *GlyT2*^{Cre} (a) and *OPN4*^{Cre} (b) mice. Density recovery profiles display density of neighboring M1 ipRGC cell bodies at distances (µm) from each soma for All M1 ipRGCs (black), non-SON projecting M1 ipRGCs (blue), and SON-projection M1 ipRGCs (magenta). M1 ipRGCs were identified morphologically. SON-projecting M1 ipRGCs = labeled from retrograde injection, non-SON projecting M1 ipRGCs = M1 ipRGCs not labeled from retrograde injection, All dorsal M1 ipRGCs = SON + non-SON projecting M1 ipRGCs. **(c)** Coverage factor ei: the proportion of dendritic overlap calculated from the average diameter of *GlyT2*^{Cre} M1 ipRGCs measured from either Neurobiotin fills (left) or calculated from the average diameter of M1 ipRGCs reported by Berson et al. 2010[2] (right). (c - Left) **(d)** Dorsal retina of M1 ipRGCs (OFF stratifying) labeled (TdTomato) by retrograde central injection (SON) in *OPN4*^{Cre} retina (open magenta circles over soma). (g – middle) M1 ipRGCs not labeled by central injection (melanopsin staining) (blue circles over soma). (g right) overlap of SON (magenta) and non-SON (blue) projecting M1 ipRGCs in the dorsal retina. Brown * = predicted as unlabeled SON projecting M1 ipRGC (GlyT2^{Cre} ipRGC) based on mosaic spacing (still considered non-SON (blue) projecting for any calculations). N = 3 retina for each strain. Area = 1mm^2. Values are mean±SEM. Scale bars: (d); 200 µm, (i,ii); 200 µm.

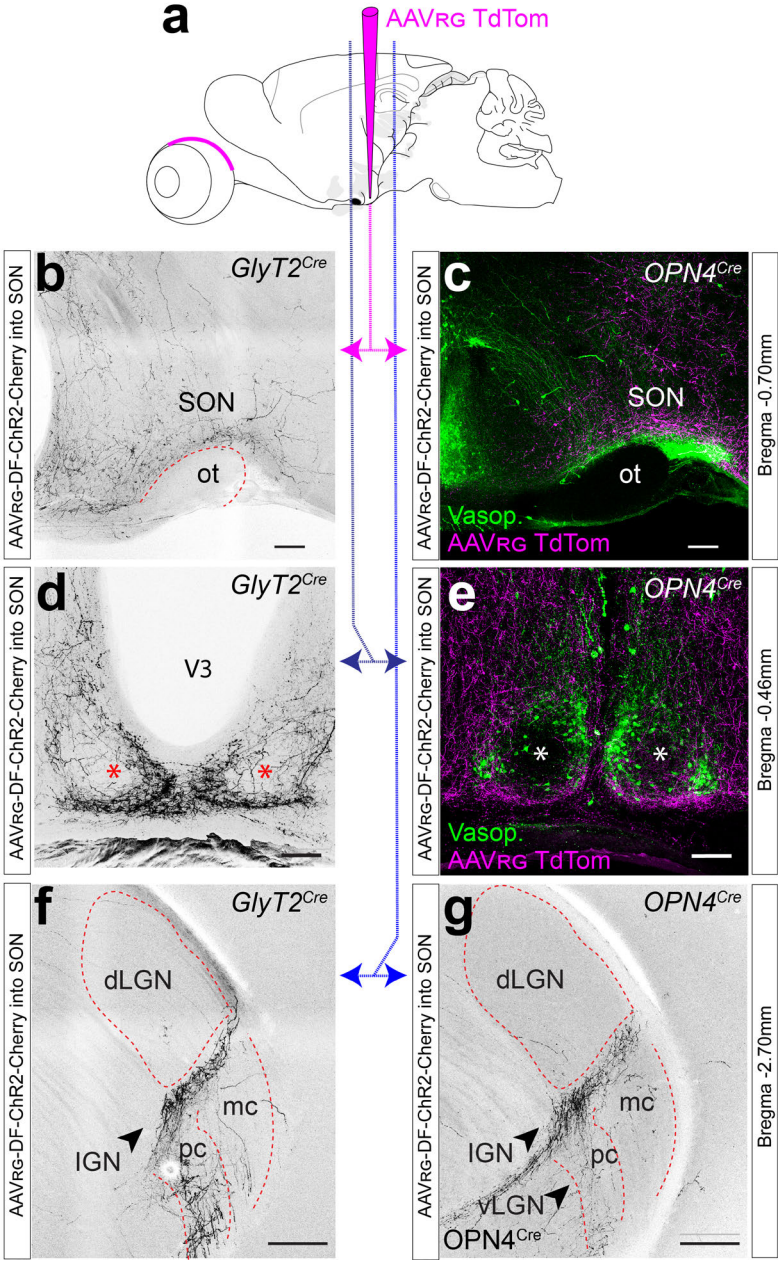

Supplementary Figure 8: SON ipRGCs have unique innervation to circadian brain regions

(a-i) Focal injections of Cre-dependent retroAAV (AAVRG-DF-ChR2-mCherry) into the supraoptic nucleus (SON) of *GlyT2*^{Cre} (left) and *OPN4*^{Cre} (right) mice. In confocal images of coronal brain slice (200um) retrograde tracing is observed in SON **(a,b)**, shell of the suprachiasmatic nucleus (SCN)**(e,f)**, and the parvocellular division (pc) and intergeniculate leaflet (IGL) (h,i) of the geniculate complex, in a projection pattern similar that observed in brain slices from anterograde eye injections in *GlyT2*^{Cre} mice (Fig. 9-13). **(c,f)** Co-stained with vasopressin (green) to aid in anatomical visualization of the SON and SCN shell. Confocal images of brain slices from anterograde eye injection of Cholera toxin subunit B (CTB) **(d,g)** provided for anatomical comparison. Distance from Bregma

determined anatomically using Franklin & Paxinos Mouse Brain Atlas. Scale bar a; 1mm, b,c; 200µm, d-f; 100µm, g-i; 250µm.

Table 1: Antibodies and immunostaining

Antibodies/Dyes	Concentration	Duration	Source	Identifier
Cholera toxin subunit B, Alexa Flour 488	1-μl IV eye injection	In vivo - 1 wk	Life Technologies Corporation	
Rabbit Anti-Melanopsin	1:2000	Retina - 3days - (rt)	ATSBio	Cat#: AB-N39
Chicken Anti-Cherry Antibody	1:1000	Retina - 3days - (rt)	Abcam	Cat#: ab205402
	1:1000	Brain slice - overnight (rt)		
Goat Anti-GFP Antibody	1:1000	Retina - 3days - (rt)	Abcam	CAT#: ab5450
	1:1000	Brain slice - overnight (rt)		
Goat Anti-Cholera Toxin subunit B	1:4000	Brain slice - over night (rt)	List Labs	Cat#: 703
Rabbit Anti-Vasopressin Antibody	1:5000	Overnight - (rt)	Immunostar	Cat#: 20069
Rabbit Anti-UV Cone Opsin Antibody	1:1000	Overnight - (rt)	Millipore	Cat#: ab5407
Rabbit Anti-SMI-32 Antibody	1:1000	Overnight - (rt)	BioLegend	Cat#: ab509997
Donkey Anti-Rabbit Alexa Flour 647	1:1000	Overnight - (rt)	Jackson Immuno Research	Cat#: 711-605-152
Donkey Anti-Goat Alexa Flour 488	1:1000	Overnight - (rt)	Jackson Immuno Research	Cat#: 705-545-147
Donkey Anti-Chicken Alexa Fluor Cy3	1:1000	Overnight - (rt)	Jackson Immuno Research	Cat#: 703-165-155

Table 2: Coverage Factors for Various ipRGC cells from GlyT2 and OPN4 mice using random intercept mixed effects models.

	Area from Fills (0.082mm^2)		Area from Berson (0.059mm^2)		
Cell Type	**GlyT2**[a]	**OPN4**[a]	**GlyT2**[a]	**OPN4**[a]	**p-value**[b]
SON M1 ipRGCs	2.17 (0.247)	2.1 (0.259)	1.56 (0.178)	1.51 (0.186)	0.851
Non-SON M1 ipRGCs	3.59 (0.247)	3.55 (0.259)	2.58 (0.178)	2.56 (0.186)	0.926
All M1 ipRGCs	5.74 (0.247)	5.63 (0.259)	4.13 (0.178)	4.05 (0.186)	0.762

[a] Values written as Mean(SE).

[b] P-values comparing means for OPN4 vs. GlyT2 coverages from t-tests using Satterthwaite's method.

1. Bleckert, A., Schwartz, G.W., Turner, M.H., Rieke, F. & Wong, R.O. Visual space is represented by nonmatching topographies of distinct mouse retinal ganglion cell types. *Current biology : CB* **24**, 310-315 (2014).
2. Berson, D.M., Castrucci, A.M. & Provencio, I. Morphology and mosaics of melanopsin-expressing retinal ganglion cell types in mice. *The Journal of comparative neurology* **518**, 2405-2422 (2010).